

Cosmic Ray Acceleration in Supernova Remnants

Olwen Carroll BSc. (Hons)

School of Physical Sciences

Dublin City University.

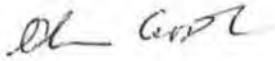
Thesis submitted for the degree of Masters of Science

Supervisor: Dr. Eamonn Cunningham

SUBMITTED OCTOBER 2002

Declaration

I hereby certify that this material, which I now submit for assessment on the programme of study leading to the award of Masters of Science is entirely my own work and has not been taken from the work of others save and to the extent that such work has been cited and acknowledged within the text of my work.

Signed: 

ID Number: 50161466

Date: 28th October 2002

Acknowledgements

Firstly, I would like to express my appreciation to Professor Luke Drury for his constant support and guidance. His shared knowledge and dedication proved to be both refreshing and inspiring.

I am also indebted to the staff of the Max-Planck Institute in Heidelberg and, in particular, to Michael Panter for the unique opportunity to part-take in the HESS project and assist in work on site in Namibia.

The staff of the School of Cosmic Physics, DIAS, deserve a special mention. In particular, Eimhear Clifton and Hilary O'Donnell for the invaluable advice and entertaining tea breaks. To John Walsh and Eric van der Swaluw for the much needed assistance with C programming. Thanks to Justin Donnelly and Jung-Kyu-Lee for the endless hours of fun in the front students room and the very amusing, if sometimes disturbing, badminton games! A special thanks to Justin and Jung-Kyu for their help, support and advice.

I would also like to express my gratitude to Eamonn Cunningham for his encouragement and support.

Finally, I would especially like to thank my family and Denis for their unwavering love and support during the trials and tribulations over this study period.

Contents

1	Cosmic Rays	1
1.1	Discovery of Cosmic Rays	1
1.2	What are Cosmic Rays?	2
1.3	Where do Cosmic Rays come from?	3
1.3.1	Galactic Cosmic Rays	3
1.4	The ^{10}Be Clock	6
1.5	The Cosmic Ray Energy Budget	8
1.6	Cosmic Rays As A Source of Gamma-Rays	9
1.6.1	Extensive Air Showers	13
2	The Evolution of a Supernova Remnant	22
2.1	Introduction	22
2.2	The freely expanding stage	23

2.2.1	The Sedov-Taylor stage	24
2.2.2	The Snowplow stage	28
3	Acceleration of Cosmic Rays	30
3.1	Introduction	30
3.2	Fermi Acceleration and the DSA Theory	31
3.2.1	First and Second order Fermi Acceleration	31
3.3	Diffusive Shock Acceleration	37
3.4	Cosmic Ray Acceleration at SNR Shocks	38
4	Models of Shock Acceleration	42
4.1	The Test Particle Theory of Shock Acceleration	42
4.1.1	Maximum Energy	43
4.1.2	The Rankine-Hugoniot Relations	45
4.2	Magnetic Field	46
4.3	Models of Shock Acceleration	47
4.4	A Box Model of Shock Acceleration	49
5	Particle acceleration in supernova remnants and the Bell-Lucek hypothesis	53
5.1	Introduction	53

5.2	The Bell-Lucek hypothesis	54
5.3	Incorporating the Bell-Lucek effect in the “box” models	56
5.4	Solution of the box equation	58
5.5	The injection rate	61
5.6	Application to the Sedov solution	63
5.7	Conclusions	67
6	Discussion and Future Work	70

List of Figures

1.1	<i>The Cosmic Ray energy spectrum below and above the “knee”</i>	20
1.2	<i>EGRET All-Sky Gamma Ray Survey Above 100 MeV</i>	21
2.1	<i>The velocity profile of a young supernova remnant (500 years old). The parameters which have been taken for this example are a total mechanical energy $E_0 = 10^{51}$ erg, the ejecta mass $M_{ej} = 1M_{\odot}$ and a uniform density $\rho_0 = 10^{-24}$ g/cm³. The corresponding transition time for these parameters equals $t_{ST} \simeq 277$ years, which means that the considered supernova remnant is in the transition region from freely expanding to the Sedov-Taylor stage. Therefore there is besides the forward shock also a reverse shock in the supernova remnant.</i>	25

2.2	<i>The radius of the forward shock of a supernova remnant. The parameters have been chosen such that the total mechanical energy $E_0 = 10^{51}$ erg, the mass of the ejecta $M_{ej} = 3M_\odot$ and the ambient hydrogen number density per cm^3 $n_0 = 1.0$. For such a supernova remnant the transition time $t_{ST} \simeq 522$ years and $t_{PDS} = 29\,000$ years.</i>	27
3.1	<i>Sketch of a collision of a charged particle with a moving magnetic cloud</i>	32
3.2	<i>Sketch of a collision of a charged particle with a moving shock . . .</i>	35
5.1	<i>Log Energy (eV) versus Log Time (years) for typical protons in the box</i>	69

List of Tables

1.1	<i>Radioactive isotopes created in spallation reactions and their half-lives.</i>	6
1.2	<i>Relative abundances of elements</i>	12

Abstract

High-energy astrophysics concerns itself with the origin of energetic particles and photons in the universe. Some astrophysical objects which have been identified as sources of energetic particles include the sun; flare stars; SNRs (supernova remnants); pulsars and AGN (active galactic nuclei)

The search for an extraterrestrial source of radiation began in 1911 when the Austrian physicist Victor Hess initiated a series of balloon flights to determine the radiation intensity variation as a function of height above the surface of the Earth. He showed that the intensity of naturally occurring radiation increases with sufficient height, which can be explained by a decreased shielding of an extraterrestrial source of radiation by the remaining column of air above the balloon. Millikan christened the observed high-energy particles Cosmic Rays (CRs) at a later date.

It is now an established fact that cosmic rays do not constitute a local phenomenon and that in fact the majority must originate from distant sources either in our own Galaxy or beyond.

The purpose of this thesis is to investigate particle acceleration at the shock fronts associated with expanding SNRs. Most models of galactic CR acceleration have focused on SNRs based on the total energy input required. The phenomenon being investigated requires a knowledge of CRs themselves – their propagation and development through the atmosphere (scattering,

collisions resulting in fragmentation into their constituent parts); shock dynamics – how a shock front is formed, jump conditions for particles across a shock front; SNRs – their formation and expansion characteristics; and also particle acceleration – acceleration times, diffusive lengths, scattering mechanisms etc.

The Bell–Lucek hypothesis, which suggests that diffusive shock acceleration (DSA), the conventional process of particle acceleration in shocks, may also result in an amplification of the highly tangled magnetic field around the shock, is investigated using the “box” model. The equations in question were solved using a C programme that solves systems of equations using the Runge–Kutta method.

Chapter 1

Cosmic Rays

1.1 Discovery of Cosmic Rays

The search for a general background source of ionizing radiation began in the early 1900s, in an attempt to explain the continuous and uncontrollable leakage of electrical charge from a well insulated gold leaf electroscope. In 1900 Father Thomas Wulf took his electroscope to the top of the Eifel Tower ($\sim 300\text{m}$ asl), and noticed a 64% decrease in the leakage rate. If the source of ionization was the radioactive material of the Earth, as was previously thought, there should have been a much more significant reduction in the ionization level due to absorption in the air. Wulf therefore concluded that the radiation from the ground, although decreasing gradually with altitude, was in competition with some form of radiation coming from gases in the

atmosphere.

In 1911, the Austrian physicist Victor Hess initiated a series of balloon flights to determine the radiation intensity variation as a function of height above the surface of the Earth. He noted that, although the intensity of ionizing radiation decreased initially with altitude, at a height of $\sim 5,000$ ft the radiation was more intense than at sea level, and at the maximum height of $\sim 16,000$ ft the intensity level had increased significantly. Hess hypothesized that the radiation responsible for ionization was extra-terrestrial in origin and subsequently (1936) received the Nobel Prize for Physics for his discovery. This penetrating radiation was given the name cosmic radiation by Millikan in 1925.

1.2 What are Cosmic Rays?

The Earth is constantly being bombarded by high energy cosmic particles – ionized nuclei which are $\sim 90\%$ protons, 9% alpha particles and other heavier nuclei. Most cosmic ray (CR) particles are relativistic and therefore ionize the media through which they pass at a rate at or near the minimum ionization ($\sim 2 \text{ MeV g}^{-1}\text{cm}^2$). Perhaps one of the most striking properties of the cosmic radiation is its wide energy range $\sim 10^9 - 10^{19}$ eV, with a few CRs even having ultrarelativistic energies extending up to 10^{20} eV. Observations have concluded that CRs consist almost exclusively of charged particles and

the fraction which consists of em radiation (e.g. γ -rays in electron-photon cascades, decay products of π^0 mesons and other transients) is of such short wavelength that particle features dominate over wavelike features.

1.3 Where do Cosmic Rays come from?

CRs are ubiquitous but their origins are surprisingly difficult to understand. It is well established however, that CRs do not constitute a local phenomenon and that in fact the majority must originate from distant sources either in our own galaxy or beyond.

1.3.1 Galactic Cosmic Rays

In general galactic CRs arrive at the top of the atmosphere uniformly from all directions – they are isotropically distributed to an accuracy of about 1 part in 10^4 . This isotropy suggests that either the particles do not come from the one region or that they have been deflected so often in their travels that they have lost all sense of their original directions of travel.

Several factors control the path of a CR – its initial direction of travel; its mass, speed and electric charge; and how the magnetic field varies with distance from the Earth. Consequently, the direction of motion changes continuously as the CR approaches the Earth and it follows a highly convoluted path.

CRs incident on the Earth's atmosphere have a spectrum which is a power-law in energy given by

$$N(E)dE = \kappa E^{-s} dE, \quad (1.1)$$

(for $E \leq 10^{15}$ eV)

There is little variation in the spectral index ($s \sim 2.7$) for energies in the range $\sim 10^{10} - 10^{15}$ eV. At greater energies however, the spectrum steepens so that $N(E) \propto E^{-3}$ up to about 10^{19} eV. At the highest energies ($E \geq 10^{19}$ eV) the CRs are believed to be extragalactic in origin. At such high energies, these particles should not be significantly influenced by the magnetic field in our galaxy and they should propagate in a relatively straight line from source to observer. Their arrival directions seem to be isotropically distributed but their origin has not yet been fully understood.

CR energy spectra near the Earth have been shaped by a complex combination of injection, acceleration and propagation. These processes are themselves modified by energy losses, collisions and possible leakage from the galaxy, and all depend on particle energies. It is now generally thought that the galactic CRs (with $E \leq 10^{19}$ eV) are accelerated at strong shocks associated with supernova remnant (SNR) blast waves in the interstellar medium (ISM). The idea of SNRs as the origin of CRs becomes more attractive when one considers that CRs below the "knee" in the spectrum roughly mirror the composition of the sun and the interstellar medium, and also when one examines the energy budget of the CRs in the galaxy.

Although the existence of the “knee” in the CR spectrum has been known for over four decades, none of the many models proposed to explain this feature has been broadly accepted. Some models focus on a possible crossover between different acceleration mechanisms below and above the “knee” (e.g. Lagage & Cesarsky 1983; Biermann 1993; Drury et al. 1994), or exploit the possibility of a change in the particle acceleration efficiency (Fichtel & Linsley 1986; Jokipii & Morfill 1986; Kobayakawa et al. 2000). Other hypothesis include the nuclear photodisintegration at the sources (Karakula & Tkaczyk 1993; Candia et al. 2002) and leakage from the Galaxy due to a change in the confinement efficiency of CRs by galactic magnetic fields (e.g. Ptuskin et al. 1993).

From the shape of the energy spectrum, most of the CR particles are those with energies below 10^{15} eV. The energy density of CRs with energies $E \geq 10^{19}$ eV is 1 eVm^{-3} (Longair), only about 10^{-6} of the total energy density of CRs. The most straightforward interpretation of this data is that the bulk of the CRs are of Galactic origin but the very highest energy particles, with $E \geq 10^{19}$ eV, may have an origin outside our Galaxy and probably within the local supercluster.

Isotope	Half-life (years)
^{10}Be	1.6×10^6
^{26}Al	7.3×10^5
^{36}Cl	3.0×10^5
^{53}Mn	3.7×10^6

Table 1.1: *Radioactive isotopes created in spallation reactions and their half-lives.*

1.4 The ^{10}Be Clock

Most nuclei assumed to be injected at CR sources are stable (nonradioactive). The most common approach to dealing with the question of a confinement timescale for CRs uses the fact that some nuclei produced in interstellar spallation reactions are radioactive and so their abundances can be used to date the CRs observed near the Earth. The longest lived of these is shown in the table above. ^{10}Be is especially interesting because of its use as a chronometer for CR travel in the galaxy.

Among the beryllium isotopes produced by the fragmentation of heavier nuclei, only ^9Be is stable, but ^{10}Be has a half-life of ~ 1.6 million years – comparable to the travel time of CRs. Radioactive nuclei start to decay immediately after creation. The ^{10}Be will undergo β -decay into ^{10}B so that the relative abundances of the isotopes of Be and B will show whether or not all the ^{10}Be has decayed and therefore provide an estimate of the mean age of the CRs detected on Earth.

In his book, Longair [52] gives a comprehensive treatment of the expected

abundance of ^{10}Be for the “leaky box” model, where the Galaxy is classified as a volume from which there is an associated escape time τ_e . He finds the steady state ratio of radioactive to non-radioactive species for the special case of ^{10}Be and ^7Be isotopes:

$$\frac{N(^{10}\text{Be})}{N(^7\text{Be})} = \frac{(1/\tau_e(^7\text{Be})) + (1/\tau_{spal}(^7\text{Be}))}{(1/\tau_e(^{10}\text{Be})) + (1/\tau_r(^{10}\text{Be})) + (1/\tau_{spal}(^{10}\text{Be}))} \frac{C(^{10}\text{Be})}{C(^7\text{Be})}, \quad (1.2)$$

where τ_e = escape time; τ_{spal} = timescale over which isotope is destroyed by inelastic collisions; τ_r = characteristic lifetime of isotope; C= production rate of the isotope. By assuming that the timescale for the destruction of the beryllium isotopes is greater than their escape times, the above relation may be simplified to obtain

$$\frac{N(^{10}\text{Be})}{N(^7\text{Be})} = \frac{(1/\tau_e(^7\text{Be}))}{(1/\tau_e(^{10}\text{Be})) + (1/\tau_r(^{10}\text{Be}))} \frac{C(^{10}\text{Be})}{C(^7\text{Be})}. \quad (1.3)$$

Several estimates of the ratio of beryllium isotopes in CRs have been made and they all correspond to an escape time of approximately 10^7 years (10 million years) and an interstellar gas density of $\sim 2 - 3 \times 10^5 \text{ m}^{-3}$. Astrophysically, the above treatment is a simplified picture of what is happening in our Solar system so that all the ^{10}Be clock can tell us is that the typical time it takes a high energy particle to travel from its source to the Earth is $\sim 10^7$ years.

1.5 The Cosmic Ray Energy Budget

There are two aspects to the question of CR acceleration – (i) what is the source of power for the accelerator; (ii) what is the actual acceleration mechanism. The measured flux of CRs show that the local CR energy density near the sun is $\rho_E \sim 1\text{eV}/\text{cm}^3$. Assuming this to be a typical value for the galaxy, and with a galactic disk volume of 10^{67}cm^3 , the total CR content is $\sim 10^{67}\text{eV} \simeq 1.6 \times 10^{55}\text{ergs}$. If a typical CR spends ~ 10 million years (3×10^{14} sec) in the galaxy before escaping into intergalactic space, the rate at which energy is lost corresponds to

$$L_{CR} \sim V_D \rho_E / \tau_R \sim 5 \times 10^{40} \text{ erg/sec.} \quad (1.4)$$

where V_D = volume of galactic disk; ρ_E = CR energy density; τ_R = CR residence time.

If the galactic CR energy is to be maintained at a steady value, this loss must be compensated by injection and acceleration of new CRs. If we take a rate of one SN every 30 years (9.47×10^8 sec) and a kinetic energy yield per event of $\sim 10^{51}$ ergs, then the average available power in SNRs is roughly 10^{42} ergs/sec. Although a rough estimate, this amount of energy is certainly sufficient to power CRs.

Identifying SNRs as likely powerhouses for CRs, and focusing on the total energy input required still leaves one major question unanswered – how is

such a large fraction of this energy directed into CRs? Before examining the injection and acceleration mechanisms of SNR shocks, I will first review the idea of CRs as a source of gamma-rays.

1.6 Cosmic Rays As A Source of Gamma-Rays

Ever since their discovery at the turn of the last century, the quest for the origin of CRs was on. Being charged particles, CRs are scattered and isotropized by the galactic magnetic field and therefore follow erratic paths, making their origins difficult to detect. If a neutral radiation like gamma-rays is associated with the presence of energetic particles in a source, they travel in straight lines and their sources can be identified.

Schlovsky pointed out in the early 1950s that the high degree of optical polarization from the Crab Nebula (a supernova remnant in the constellation Taurus due to a supernova explosion in 1054 AD), could be accounted for by a synchrotron process requiring the presence of very high energy ($> 10^{12}\text{eV}$) electrons gyrating around magnetic fields ($\sim 10^{-4}\text{G}$) in the filaments of the nebula. In 1960, Cocconi [18] suggested that since electrons of such high energy cannot arise from nuclear decay processes, a mechanism of acceleration of particles to high energies must be operating in the nebula. If such a mechanism was present, there was no reason why protons could not be

accelerated to high energies too. The presence of such high energy protons meant that charged and neutral pions could be created in collisions with the nebular matter. The decay of such high energy neutral pions results in the production of high energy (hundreds of GeV) gamma-rays. Therefore, detection of high energy gamma-rays leads to the discovery of CR sources.

SNRs (supernova remnants) have long been invoked as a principal source of galactic CRs, created via the process of diffusive Fermi acceleration at their expanding shock fronts (e.g. Drury 1983; Lagage & Cesarsky 1983). The best way to test this hypothesis is to search for the gamma-ray signal produced by the interaction of the CR population with the remnant environment. In the case of hadrons, this signal is produced by pions from nuclear collisions; in the case of leptons, by Bremsstrahlung or inverse Compton scattering of the cosmic microwave background radiation (CMBR). Such a signal should indicate that the nuclear component of CRs in SNRs is much younger than that in the ISM (interstellar medium) or, failing this, that it is much more intensive in SNRs than in the ISM.

The concept of gamma-ray emission was explored by Drury, Aharonian & Völk (1994). In their model, the gamma-ray luminosity is spawned by collisions between the CRs and nuclei from the ambient SNR environment. Models of Mastichiadis and de Jager (1996), Gaisser, Protheroe and Stanev (1997), and Sturmer et al. (1997) suggest that ee (electron-electron) and ep (electron-proton) Bremsstrahlung and inverse Compton scattering involving

shock-accelerated electrons interacting with the CMBR and also IR/optical emission from dust/starlight form added components.

Just as Galactic radio emission outlines the distribution of high energy electrons in magnetic fields in the Galaxy, so the distribution of gamma-radiation can provide information about high energy protons and the overall distribution of the interstellar gas.

Collisions between high energy particles and protons and nuclei of atoms and molecules of the interstellar gas produce pions of all charges π^+ , π^- , π^0 . The positive and negative pions decay into positive and negative muons which, in turn decay into positrons and electrons with relativistic energies. The latter may make a contribution to the low energy electron spectrum. The neutral pions decay almost instantly into two γ -rays. In proton-proton collisions, the cross-section for the production of a pair of high energy γ -rays is roughly the geometric proton size, $\sigma_\gamma \approx 10^{-30} \text{m}^2$. The characteristic signature of the spectrum of γ -rays produced in this process, is that they have a broad maximum at about 70 MeV. To produce TeV gamma-rays through hadronic processes, protons will have to be accelerated to at least 10 TeV. This is also the energy that electrons require to produce TeV gamma-rays by inverse Compton scattering of the CMBR.

In his book, Gaisser [30] develops an expression for the ratio of Bremsstrahlung

Elements	Cosmic Rays	Sun
H	1	1
He	0.1	0.01
Z>2	0.03	≈0.001
Electrons	≪ 10 ⁻²	1

Table 1.2: *Relative abundances of elements*

photons to π^0 photons for power law spectra at high energies ($E_\gamma \gg 70$ MeV):

$$\frac{e \rightarrow \gamma}{\pi^0 \rightarrow \gamma} = \left[\frac{1}{N_A X_0 \sigma_{pp}^{inel}} \right] \left[\frac{\alpha}{2Z_{N \rightarrow \pi^0}} \left(\frac{1}{\alpha + 1} + \frac{1.35}{\alpha - 1} - \frac{1.35}{\alpha} \right) \right] \left[\frac{\phi_e}{\phi_N} \right] \quad (1.5)$$

This is $\simeq [0.85][27 \times (0.6)] \left[\frac{\phi_e}{\phi_N} \right]$

where X_0 =radiation length; σ_{pp}^{inel} =cross section for proton-proton inelastic collisions; α =spectral index; ϕ_e =spectrum of electrons; ϕ_N =spectrum of nucleons.

The first term on the right represents the ratio of interaction lengths for the two processes, which is about one. The second factor is the ratio of the spectrum weighted moments of the inclusive cross-sections. The third term is the ratio of the electron and CR nucleon spectrum.

An examination of the table above, of the relativistic abundances of various elements, reveals that there are practically no electrons in the CRs. Since electrons should also be produced in the processes which give rise to the protons, their absence must somehow be explained. The relativistic electrons which we can expect to be produced along with other particles that are

actually observed in CRs are responsible for the radio frequency emissions observed in radio astronomy. The electrons lose their energy by magnetic Bremsstrahlung while getting accelerated by the interstellar magnetic fields.

1.6.1 Extensive Air Showers

The discovery of air showers is generally attributed to Pierre Auger (1938) who, along with his colleagues in France, was studying coincidences in a CR telescope. They noted that they were recording coincidences between counters separated horizontally by distances of up to 75 meters. As early as 1934 however, Bruno Rossi had noticed coincidences between several counters placed in a horizontal plane, far in excess of chance coincidences. Before going into further details, let us first examine the cascade process which leads to such particle showers.

When a primary CR proton or nucleus enters the Earth's atmosphere, it interacts strongly with a nucleus in the air (e.g. Nitrogen, Oxygen). In such high energy collisions, part of the primary particle energy is lost in the production of secondary particles (mesons, baryons, hyperons etc.). The energy lost by the primary nuclei is shared by the secondaries and the number of secondaries slowly increases with the energy of the interaction.

The majority of particles produced in the first interaction are pions. These particles interact even further in the air as they travel down and produce even more particles but of lower energy. These particles in turn interact or

decay further down in the atmosphere and this “nuclear cascade” propagates downwards.

Some of the particles produced in the cascade are neutral pions, which decay almost immediately into two γ -rays by the following reaction:

$$\pi^0 \rightarrow \gamma + \gamma. \quad (1.6)$$

The gamma-rays initiate electromagnetic cascades. The products of these cascades are photons, electrons and positrons, and they constitute the electromagnetic component of air showers. The charged mesons give rise to muons (μ mesons) when they decay:

$$\pi_{\pm}^{\pm} \rightarrow \mu_{\pm}^{\pm} + \nu \quad (1.7)$$

$$K_{\pm}^{\pm} \rightarrow \mu_{\pm}^{\pm} + \nu \rightarrow \pi_{\pm}^{\pm} + \pi^0 \quad (1.8)$$

The neutrinos formed above only have weak interactions and therefore manage to escape, carrying a significant fraction of the primary energy. The surviving hadrons, all strongly interacting particles such as pions, kaons, hyperons etc., form the hadronic component of the shower.

As the shower propagates down through the atmosphere, the hadron and electromagnetic components increase in size, reach a maximum and then decrease. The muon component however does not suffer significant attenuation after reaching maximum, therefore muons only lose energy by ionization and

a small fraction of them are lost by decay. This complex nuclear electromagnetic cascade is called an Extensive Air Shower (EAS).

Properties of air showers are generally studied as a function of shower size. Thus, the first task in the analysis of air shower data is to determine the shower size. Traditionally this is done by fitting the observed particle densities in various detectors to an assumed lateral distribution function in the shower plane. The shower plane, which is perpendicular to the direction of the primary particle, also called the shower axis, is determined from the relative arrival times of the particles recorded in various detectors. The shower axis is characterized by the zenith and azimuth angles in the local coordinate system.

Many air shower arrays employing the above technique have been constructed worldwide e.g. SPASE (South Pole Air Shower Experiment) operational since 1987 and the Tibetan Air Shower Array at an altitude of 4300 m and in operation since 1990.

The array of four (Phase I) IACTs (Imaging Atmospheric Cerenkov Telescopes) of the HESS project detects the Cerenkov light emitted by particles travelling through the atmosphere. Cerenkov light is emitted by a charged particle travelling in a dielectric medium with velocity greater than the speed of light in the medium. The light is emitted at an angle θ with respect to

the direction of motion of the particle given by:

$$\cos \theta = \frac{1}{\beta n}, \quad (1.9)$$

where $\beta = \frac{v}{c}$; v = particle velocity; c = light velocity; n = refractive index of medium. Only particles with $\beta > \frac{1}{n}$ can emit Cerenkov light, thus setting a threshold energy. The light is emitted along the surface of a cone of half angle θ around the direction of the particle.

The Cerenkov technique differs fundamentally from other EAS techniques on a variety of counts. Firstly, because it is the atmosphere itself which is the detecting medium, the detector has ill-defined boundaries but vast dimensions. Secondly, since by nature Cerenkov radiation is directional in character, it is possible to achieve high angular resolution with equipment having quite simple optics. Thirdly, as a direct result of the first point, and because of the large area of the “light pool” illuminating the ground, the effective area of the detector is many orders of magnitude larger than the physical area of the instrument, resulting in a great reduction in cost relative to conventional arrays for the same counting rate for showers of comparable energy. Finally, the most distinguishing feature of the Cerenkov technique is that whereas all other EAS equipments yield information mainly about the lateral distributions of particle energies and densities, and then only for the particular atmospheric level at which the array is situated, the Cerenkov technique yields information on the history of showers in depth.

High energy γ -rays entering the Earth's atmosphere develop pure electron-photon cascades, the features of which differ somewhat from the more familiar nucleon-induced showers. The γ -induced EAS contain a much smaller fraction of muons and nuclear active particles and also develop more rapidly so that, for a given primary energy E_0 , the region of maximum development occurs at a greater altitude.

The potential of the Cerenkov technique in the field of γ -ray astronomy lies essentially in the high counting rate of relatively low energy showers in a restricted field of view with installations operated on the ground. The advantages of the Cerenkov technique in the search for point sources were appreciated early on (e.g. Galbraith & Shelley 1955) while the application of the technique to the detection of γ -ray induced EAS was first suggested by Zatsepin & Chudakov (1961) and was also discussed by Jelley & Porter (1963).

Since the mean life of a charged-particle CR stored in a galactic magnetic field is long compared to the time for a γ -ray to traverse a comparable linear distance, it follows that even if γ -rays are produced at the same rate as normal CR, their apparent flux $\phi(\gamma)$ at the Earth is expected to be smaller than the nucleon flux $\phi(N)$. This low value for the γ -ray flux compared to the charged-particle primary flux presents a problem with the Cerenkov technique, in that with photomultiplier systems it is difficult to distinguish between EAS induced by γ -rays and charged particles. This problem can

be overcome using the angular spread method/Cerenkov imaging technique, developed by the Whipple group.

The Whipple collaboration constructed a 10 m diameter reflector at the focal plane of which a camera head was mounted. The camera head consists of 91 pixels of 0.25° (2.5 cm diameter phototubes) surrounded by an outer ring of 18 pixels of 0.5° (5 cm diameter phototubes) arranged hexagonally, giving a full field of view of 3.75° diameter. The effective energy threshold is ~ 0.3 TeV and the collection area for γ -ray showers is $\sim 3 \times 10^4$ m².

In gamma-ray showers, the angular spread of Cerenkov photons is solely due to the Cerenkov emission angle and the multiple Coulomb scattering of electrons that emit the light. In the case of proton showers, the opening angles of the π^0 mesons, due to the transverse momentum they acquire at production in nuclear interactions, also contribute to the spread. Therefore the angular spread of the photons, and hence the size of the Cerenkov image in angular space, is larger for proton showers than for γ -ray showers. This effect also leads to flatter lateral distribution of Cerenkov light in γ -ray showers compared to proton showers, with a characteristic hump ~ 140 m from the core. This hump is absent in proton showers.

The compact angular size of Cerenkov images due to γ -ray showers from a point source, coupled with the elliptical shape of the images, with the major axis pointing towards the center which is the direction of the source, give a single parameter “azwidth”. This is the width of the image perpendicular

to the radial axis through the image centroid. By making a suitable cut on this parameter, on the basis of Monte Carlo simulations, the Whipple group showed that γ -ray showers could be selected with at least 50% efficiency, while rejecting 97% of the background CR showers.

The predicted flux of TeV gamma-rays produced by the hadronic component of CRs from the number of nearby SNR lies near the sensitivity limit of present day ICTs. However, the only detections reported to date are of objects where energetic leptons are equally plausible as radiating particles. Those objects in which hadrons are expected to dominate have not yet shown emission at the level hoped for. However, the arguments in favour of the origin of (hadronic) CRs in SNR, principally the energy budget, remains convincing and it is hoped that such emission will be observed with the new generation of telescopes.

Next I will examine the basic concepts involved in the formation and expansion of SNRs.

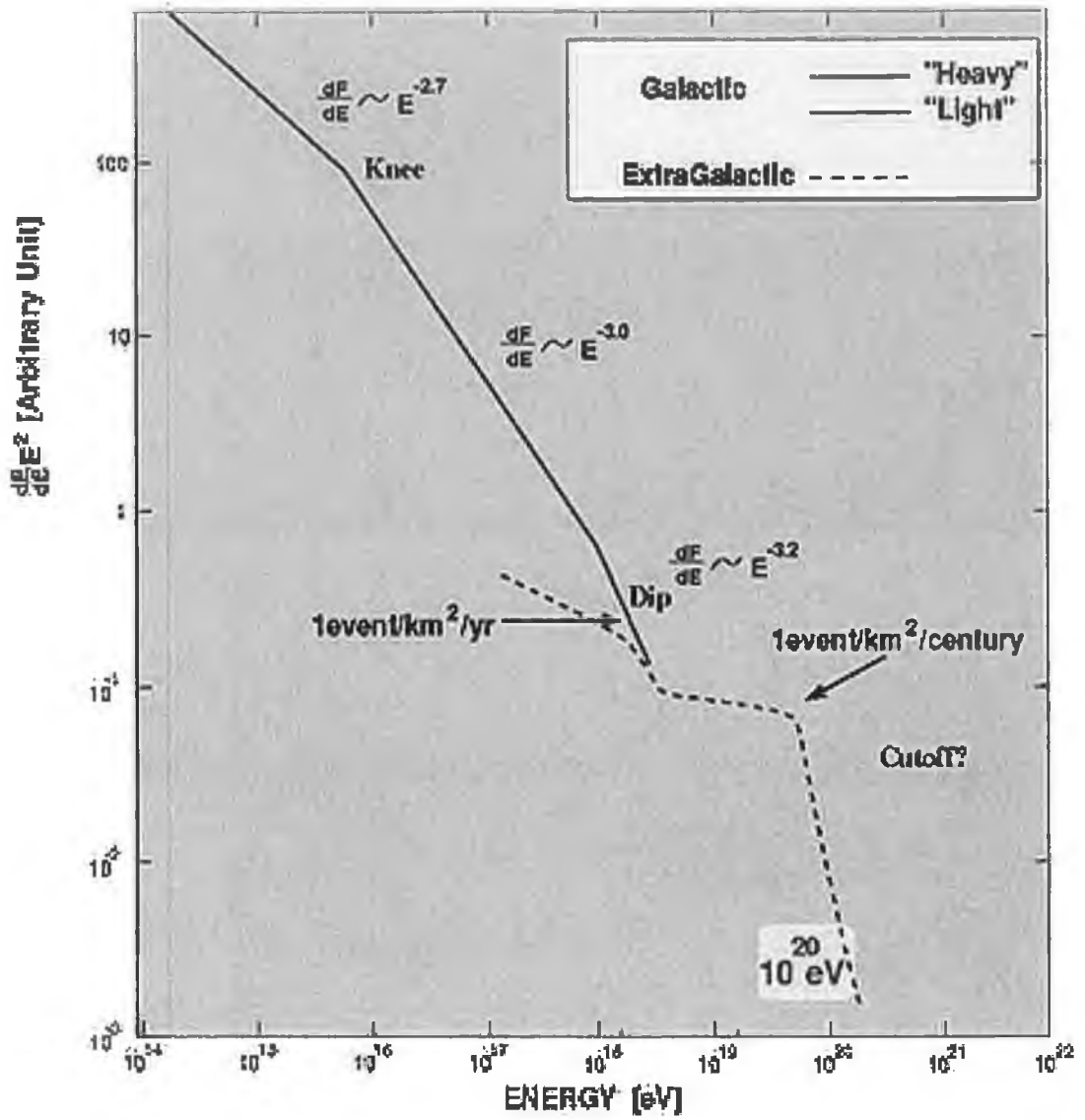


Figure 1.1: The Cosmic Ray energy spectrum below and above the “knee”

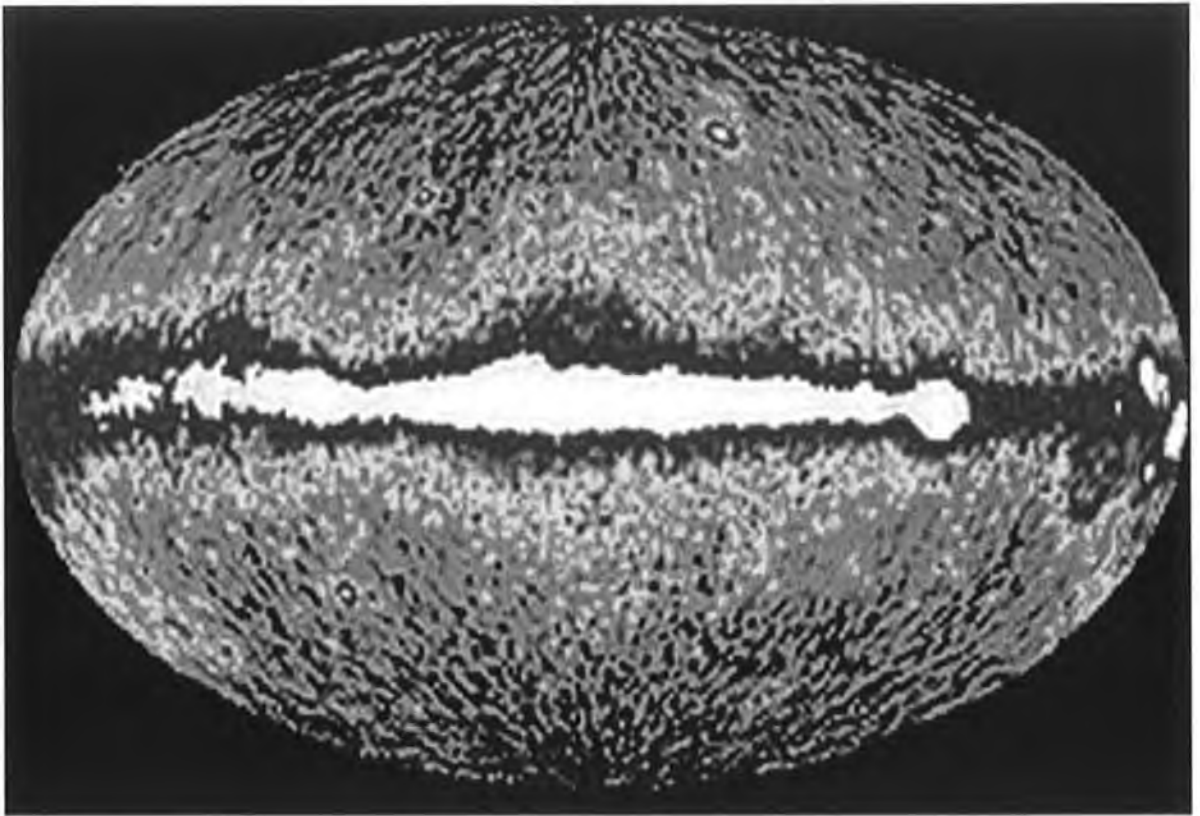


Figure 1.2: *EGRET All-Sky Gamma Ray Survey Above 100 MeV*

Chapter 2

The Evolution of a Supernova Remnant

2.1 Introduction

There are two main categories of supernova. Type I supernovae are somewhat more abundant and have greater luminosities than those of Type II and their brightness diminishes more quickly. Their properties are remarkably uniform, with essentially identical light curves and intrinsic luminosities. Type II supernovae exhibit a much more diverse range of properties.

Type I supernovae are thought to occur in the late stages of evolution of a binary system, where two stars move in orbit around each other. One of the stars is a white dwarf which accretes matter from its binary companion.

Once the mass of accreted matter exceeds the theoretical limit for the mass of a white dwarf, the Chandrasekhar limit, at close to 1.4 Solar masses, the star collapses, liberating $\sim 10^{53}$ ergs, as a neutron star with a mass of $\sim 1M_{\odot}$ is formed. The fact that the progenitor stars are all of the same type and mass accounts for the observed uniformity of their properties.

In contrast, Type II supernovae represent the final stages in the evolution of stars appreciably more massive than the sun ($M > 8M_{\odot}$). The energy release associated with a supernova explosion is typically of the order $E_{\text{sn}} \sim 10^{53}$ erg. Approximately 99% of this energy is radiated away in the form of neutrinos. The remaining 1% of the energy ($E_{\text{snr}} \sim 10^{51}$ erg) is contained in the ejected material which ultimately drives a shock wave in the surrounding medium. This results in an expanding shell containing hot shocked (swept-up) material which bounds the supernova remnant (SNR). The evolution of a SNR can roughly be divided into four stages (Woltjer 1972): the free expansion stage, the Sedov-Taylor stage, the pressure-driven snowplow stage and the momentum conserving stage. I will discuss each of these stages in this chapter.

2.2 The freely expanding stage

In the free expansion stage, the SNR consists mostly of the freely expanding (stellar) ejecta bounded by a strong shock. The total mass of the SNR

roughly equals the mass of the (stellar) ejecta M_{ej} and almost all the mechanical energy E_{snr} has been converted into kinetic energy at the start of this stage. Therefore the expansion velocity of a SNR during this stage is approximately constant:

$$V_{\text{snr}} \simeq \sqrt{2E_{\text{snr}}/M_{\text{ej}}} \sim 10\,000 \text{ km/s.} \quad (2.1)$$

A SNR will be significantly decelerated when the swept-up material roughly equals the total ejected mass during the supernova explosion event— a transition will take place to the Sedov-Taylor stage.

2.2.1 The Sedov-Taylor stage

The transition from the free expansion stage to the Sedov-Taylor stage takes place after a few ~ 100 years, when the total swept-up mass from the ISM exceeds the ejected mass during the supernova explosion event. McKee & Truelove (1995) give a typical timescale for this transition time:

$$t_{\text{ST}} \simeq 209 E_{51}^{-1/2} \left(\frac{M_{\text{ej}}}{M_{\odot}} \right)^{5/6} n_0^{-1/3} \text{ yr.} \quad (2.2)$$

Here E_{51} is the total mechanical energy of the SNR in units of 10^{51} erg, M_{ej} is the ejecta mass and n_0 is the ambient hydrogen number density assuming the typical interstellar composition of 10 H: 1 He ($n_0 = \rho_0/2.34 \times 10^{-24}$ g). At the end of the free expansion stage a reverse shock is driven deep into

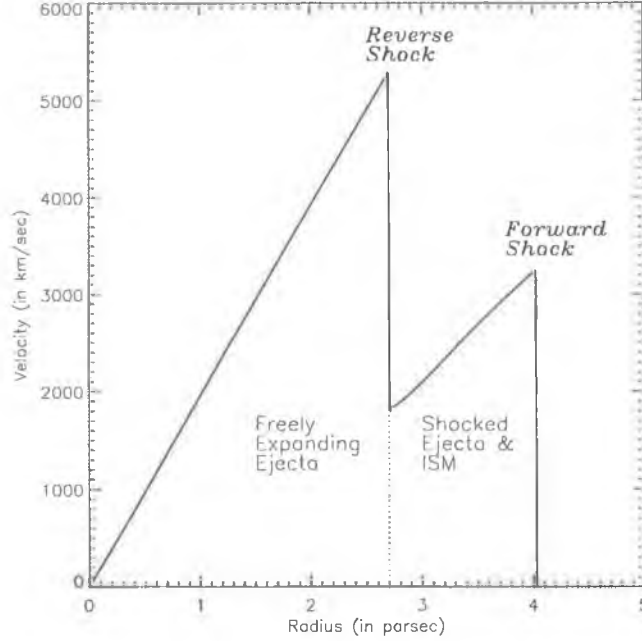


Figure 2.1: *The velocity profile of a young supernova remnant (500 years old). The parameters which have been taken for this example are a total mechanical energy $E_0 = 10^{51}$ erg, the ejecta mass $M_{ej} = 1M_{\odot}$ and a uniform density $\rho_0 = 10^{-24}$ g/cm³. The corresponding transition time for these parameters equals $t_{ST} \simeq 277$ years, which means that the considered supernova remnant is in the transition region from freely expanding to the Sedov-Taylor stage. Therefore there is besides the forward shock also a reverse shock in the supernova remnant.*

the interior of the SNR (Mc Kee 1974) which will (shock-)heat the freely expanding ejecta (see also Figure 2.1).

During the Sedov-Taylor stage the SNR is bounded by a strong shock and radiative losses are negligible, therefore the total mechanical energy of the remnant is constant, i.e. $E_{snr} = E_0$. The SNR expansion law during this

stage can be derived using an energy argument. The mass of the SNR is

$$M(t) = \frac{4}{3}\pi\rho_0 R_{\text{snr}}^3. \quad (2.3)$$

Here one assumes a uniform density, i.e. $\rho_0 = \text{constant}$. The total energy can be expressed as the sum of the kinetic and thermal energies, which yields:

$$E_{\text{snr}} = E_0 = \frac{1}{2}Mu^2 + \frac{4}{3}\pi R_{\text{snr}}^3 \frac{P_{\text{snr}}}{\gamma - 1}, \quad (2.4)$$

where γ is the specific heat ratio of the gas. The value for u , the velocity behind the blastwave, and P_{snr} , the pressure behind the blastwave, follows from the Rankine-Hugoniot jump conditions in the limit of a strong shock, which yields:

$$u = \frac{2}{\gamma + 1} \frac{dR_{\text{snr}}}{dt}, \quad (2.5)$$

and

$$P_{\text{snr}} = \frac{2}{\gamma + 1} \rho_0 \left(\frac{dR_{\text{snr}}}{dt} \right)^2. \quad (2.6)$$

Substituting equations (2.5) and (2.6) into equation (2.4) yields:

$$E_0 = C_\gamma M(t) \left(\frac{dR_{\text{snr}}}{dt} \right)^2, \quad (2.7)$$

where

$$C_\gamma = \frac{4\gamma}{(\gamma - 1)(\gamma + 1)^2}. \quad (2.8)$$

Finally, using equations (2.3) and (2.7), one can derive an equation which

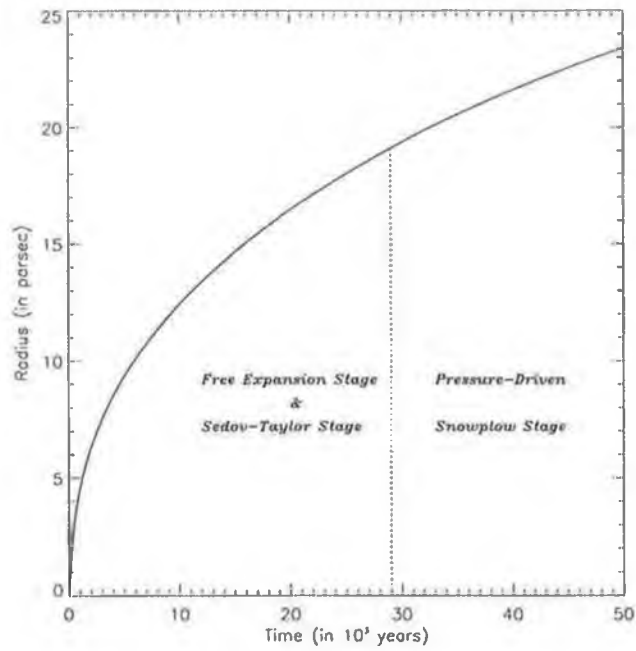


Figure 2.2: The radius of the forward shock of a supernova remnant. The parameters have been chosen such that the total mechanical energy $E_0 = 10^{51}$ erg, the mass of the ejecta $M_{ej} = 3M_{\odot}$ and the ambient hydrogen number density per cm^3 $n_0 = 1.0$. For such a supernova remnant the transition time $t_{ST} \simeq 522$ years and $t_{PDS} = 29\,000$ years.

yields an approximation for the radius of a SNR in the Sedov-Taylor stage:

$$R_{\text{snr}}(t) = \xi_0 \left(\frac{E_0 t^2}{\rho_0} \right)^{1/5}, \quad (2.9)$$

where

$$\xi_0 = \left(\frac{75(\gamma - 1)(\gamma + 1)^2}{64\pi\gamma} \right)^{1/5}. \quad (2.10)$$

In the case of a SNR, the specific heat ratio of the gas is usually taken to be $\gamma = 5/3$, which yields $\xi_0 \simeq 1.01$. One can obtain a full solution for the Sedov-Taylor expansion stage by solving the equations of gas dynamics. This yields the same equation for the radius of a SNR as in the approximation but with a different coefficient, i.e. $\xi_0 \simeq 1.15$.

2.2.2 The Snowplow stage

The snowplow stage starts when a significant fraction of the mechanical energy of the SNR has been radiated away. This transition occurs roughly when the temperature of the shell of the remnant drops below $T \sim 10^6$ Kelvin. Blondin et al. (1998) give a typical timescale for the start of this stage of the SNR evolution, i.e.:

$$t_{\text{PDS}} = 2.9 \times 10^4 E_{51}^{4/17} n_0^{-9/17} \text{ yr}. \quad (2.11)$$

Here the same notation is used as for equation (2.1) of this chapter. Following Cioffi et al. (1988), one can write the radius of the SNR in the snowplow stage as:

$$R_{\text{snr}}(t) = R_{\text{PDS}} \left(\frac{4}{3} \frac{t}{t_{\text{PDS}}} - \frac{1}{3} \right)^{3/10}. \quad (2.12)$$

Here we have taken the radius of the SNR at the transition time in the equation for the Sedov-Taylor expansion stage:

$$R_{\text{PDS}} = 1.15 \left(\frac{E_0}{\rho_0} \right)^{1/5} t_{\text{PDS}}^{2/5} = 18 E_{51}^{5/17} n_0^{-7/17} \text{ pc}. \quad (2.13)$$

At the end of the remnant's life, the expansion speed becomes similar to the local sound speed. During this stage the SNR will merge with the ISM.

Chapter 3

Acceleration of Cosmic Rays

3.1 Introduction

The question of how, where and when CRs are accelerated is most important for galactic, solar and anomalous CRs. We should note at this stage that only charged particles can be accelerated. Thus, e.g. energetic solar neutrons sometimes detected during solar flares are secondaries.

When we consider the energy distribution of CRs, as well as their composition, rate of production and other details, the task of modelling their production and propagation becomes very sophisticated. There is now broad consensus that galactic CRs are accelerated from the ISM at SNR blast waves by the diffusive shock acceleration (DSA) process. Beyond this simple statement however, significant differences of opinion quickly surface on almost

every detail and these have yet to be overcome.

3.2 Fermi Acceleration and the DSA Theory

In order to explain the origin of CRs, Enrico Fermi (1949) suggested an effective mechanism of particle acceleration. He exploited the idea of moving magnetic clouds in the ISM. These clouds have a density ~ 10 -100 times higher than the average ISM density and carry a “frozen-in” magnetic field. The Fermi acceleration mechanism is particularly attractive as it produces a spectrum of CRs close to what is observed. The most straightforward physical realisation of regular Fermi acceleration is DSA. This acceleration mechanism occurs when charged particles are scattered repeatedly across a strong shock propagating in a magnetised plasma. In the following sections I will outline the basic principles of first and second order Fermi acceleration and their application to the DSA process at SNR shocks.

3.2.1 First and Second order Fermi Acceleration

The fact that galactic CRs are undergoing a random walk immediately implies that something is scattering them. Ordinary collisions between CRs and ions in the interstellar gas are totally ineffective in scattering the CRs. It is believed that the scattering mechanism responsible for their random walk is provided by the irregularities in the galactic magnetic field. This is a

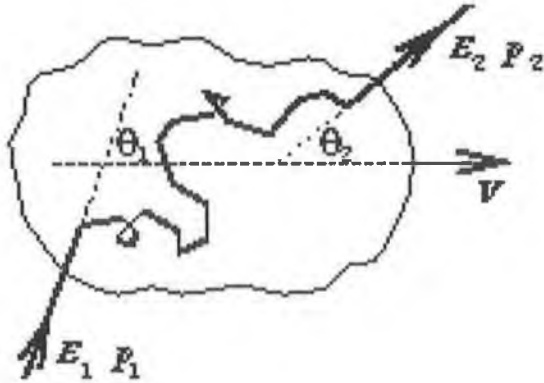


Figure 3.1: *Sketch of a collision of a charged particle with a moving magnetic cloud*

collective process in the sense that the CRs are not scattered by the em-field of a single particle in the ISM, but by a wave supported by the plasma as a whole.

A CR enters a cloud and scatters off irregularities in the magnetic field which is tied to the cloud because it is partly ionized. In the frame of the cloud, there is no energy change because the scattering is collisionless and there is elastic scattering between the CR and the cloud.

Consider a fast moving particle with energy E_1 and momentum p_1 entering a cloud at an angle θ_1 to the cloud's direction. (See Fig 3.1). Assuming the particle to be relativistic ($E \sim pc$) we get:

$$E'_1 = \gamma E_1 (1 - \beta \cos \theta_1) \quad (3.1)$$

where $\beta = V/c$ and $\gamma = 1/\sqrt{1 - \beta^2}$ are the β and Lorentz factors of the

cloud respectively, and the primes denote quantities measured in the cloud rest frame. After scattering inside the cloud, the particle emerges with an energy E_2 and momentum p_2 at an angle θ_2 to the cloud's direction. Going back to the laboratory frame, we obtain:

$$E_2 = \gamma E_2' (1 + \beta \cos \theta_2') \quad (3.2)$$

Our assumption that there are no collisions with the matter but only elastic scattering on the magnetic field leads to conservation of the particle's energy in the rest frame of the moving cloud so that:

$$E_1' = E_2', \quad (3.3)$$

from which the fractional change in energy, $(E_2 - E_1)/E_1$, follows:

$$\frac{\Delta E}{E} = \frac{1 - \beta \cos \theta_1 + \beta \cos \theta_2' - \beta^2 \cos \theta_1 \cos \theta_2'}{1 - \beta^2} - 1. \quad (3.4)$$

Because the particle motion inside the cloud is random, all possible values of θ_2' have equal probability, which leads to $\langle \cos \theta_2' \rangle = 0$. Because of the movement of the cloud, the probability of a particle entering the cloud at θ_1 is proportional to $c - V \cos \theta_1$ for relativistic particles, which gives $\langle \cos \theta_1 \rangle = -1/3\beta$. Therefore

$$\frac{\Delta E}{E} = \frac{1 + 1/3\beta^2}{1 - \beta^2} - 1 \approx 4/3\beta^2. \quad (3.5)$$

From this we see that the net energy gain averaged per collision, is $\frac{\Delta E}{E} \propto \beta^2$ and that although positive, the average energy gain is small. This is because particles can either gain or lose energy in a given encounter, depending on the angles, but after many encounters there is a net gain. Many authors explain this by suggesting that the number of head-on collisions, where a particle gains energy, exceeds the number of overtaking collisions resulting in an energy loss. In his book, Gaisser [30] disputes this idea, saying that a head-on collision with a cloud in which the particle goes out the back side ($\cos \theta'_2 < 0$) can result in a loss of energy. Likewise an overtaking collision may result in an increase in particle energy. In any case, the second order process described above does not lead to very efficient particle acceleration. Krymsky (1977), Axford et al. (1977), Bell (1978) and Blandford & Ostriker (1978) independently showed that first order Fermi acceleration by SNR shocks is particularly efficient because the motions are not random.

A charged particle ahead of the shock front can pass through the shock and then be scattered by magnetic inhomogeneities behind the shock. Consider a plane shock front moving with velocity $-u_1$ (See Fig 3.2). The shocked gas flows away from the shock with a velocity relative to the shock front, and $|u_2| < |u_1|$. Therefore, in the laboratory frame the gas behind the shock moves with velocity $V = -u_1 + u_2$. By considering the rate at which

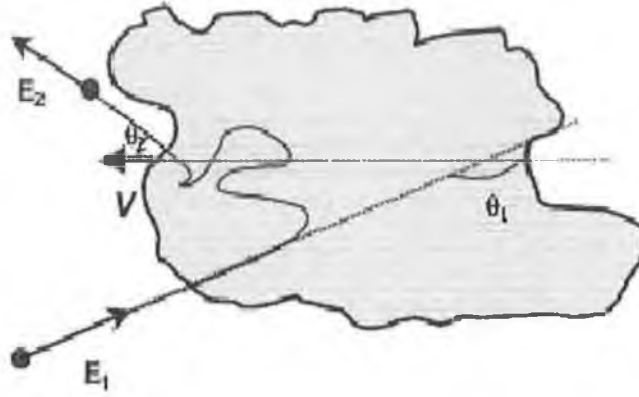


Figure 3.2: Sketch of a collision of a charged particle with a moving shock

CRs cross the shock from downstream to upstream and back, we see that $\langle \cos \theta_1 \rangle = -2/3$ and $\langle \cos \theta_2 \rangle = 2/3$ which leads to:

$$\frac{\Delta E}{E} = \frac{1 + 4/3\beta + 4/9\beta^2}{1 - \beta^2} - 1 \approx \frac{4}{3}\beta. \quad (3.6)$$

The particle gains energy and flies back across the shock where it can be scattered by magnetic inhomogeneities ahead of the shock. This enables the particle to bounce back and forth across the shock, gaining energy each time, a much more efficient acceleration mechanism than the second order described above.

Due to efficient scattering, particles can cross the shock repeatedly before

being advected downstream. A particle gains energy each time it crosses the shock in a cycle from downstream \rightarrow upstream \rightarrow downstream and the average momentum gain per cycle is given by:

$$\frac{\Delta p}{p} = \frac{4U_1 - U_2}{3c}, \quad (3.7)$$

where $U_{1(2)}$ is the fluid velocity upstream (downstream). The particles have a finite chance of escape from the confines of the shock which can be expressed as

$$P_{esc} \simeq \frac{4U_2}{c} \ll 1. \quad (3.8)$$

The resulting power law distribution in momentum of accelerated particles has a number density with slope s where:

$$s = 1 + \frac{\text{escape rate}}{\text{acceleration rate}} \quad (3.9)$$

This can be expressed as a function of the compression ratio r ($r = \rho_2/\rho_1 = U_1/U_2$) of the shock ($r = 4$ for strong shocks).

$$s = \frac{r+2}{r-1} = 2 \quad (3.10)$$

for a strong shock.

3.3 Diffusive Shock Acceleration

The fundamental assumption of the theory of diffusive shock acceleration (DSA) is that accelerated particles diffuse in space. There are numerous approaches to understanding the physics of DSA, since the microphysics is complex and depends on assumptions made about such details as the structure and orientation of the local magnetic field. However, all approaches depend on a number of nonthermal particles becoming trapped by scattering around a shock front, so that they may tap into the energy flow through the shock for extended times, but with a finite possibility of escape.

For DSA to work, the particle distribution should be almost isotropic and the particles themselves should have speeds that are large compared to the bulk flow speed u . The diffusion-convection equation which describes the time evolution of the particle distribution $f(p, x, t)$ can be expressed as

$$\frac{\partial f}{\partial t} + u \cdot \nabla f = \frac{1}{3} p \frac{\partial f}{\partial p} (\nabla \cdot u) + \nabla \cdot (\kappa \nabla f) + Q, \quad (3.11)$$

where the first term on the right represents adiabatic compression, the second spatial diffusion and Q is a generic source term that can represent injection or escape.

One of the key questions to understanding the efficiency of DSA of CRs is the injection process from thermal particles. When particles diffuse off the moving scattering centres in a region divided by a shock, these particles can

be accelerated if their mean free paths exceed the shock thickness. The relative momentum gain for a cycle of two shock crossings is then proportional to the velocity difference across the shock - of first order with respect to the shock velocity (Bell 1978). It was realized (e.g Bell 1978; Skilling 1975; Lucek & Bell 2000) that accelerated particles must create the scattering environment by themselves, generating Alfvén waves via the cyclotron instability, so that even if there are not enough irregularities to begin with, especially upstream of the shock, scattering waves can be self-generated by CRs diffusing upstream. These waves are then amplified by the shock and advected downstream where they are responsible for scattering and therefore diffusion, an essential element of the first order Fermi acceleration process.

The question of how particles might be accelerated from the thermal pool up to an energy where they can be assumed to diffuse is referred to as the injection problem and is in itself highly non-linear. This problem is fundamentally related to the question of the efficiency of particle acceleration at shocks by the Fermi process.

3.4 Cosmic Ray Acceleration at SNR Shocks

It is a reasonable assumption that it is the forward shocks in the Sedov phase of SNR expansion that are mainly responsible for the production of CRs. Although we have identified the existence of reverse shocks in the

early phases of remnant expansion, the forward shocks are much longer lived and have higher energies. Also, the CRs accelerated when the remnant is small suffer strong adiabatic losses, making later stages more important (e.g. Drury and Keane 1995).

One of the most important parameters of Fermi acceleration at an SNR shock is the rate at which it operates. The rate of energy gain of relativistic particles at a non-relativistic shock is given by

$$\frac{dE}{dt} = \frac{\Delta E}{t_{cycle}}, \quad (3.12)$$

where t_{cycle} is the time for one complete cycle i.e. crossing the shock from upstream to downstream, diffusing back towards the shock and crossing from downstream to upstream before finally returning to the shock.

In order to be accelerated efficiently, particles must interact with the shock a number of times and a downstream particle must be able to diffuse back to the shock. The acceleration rate at the shock front depends on the particle diffusion coefficient κ . This in turn depends on the particle energy through their Larmor radius and the properties of the plasma turbulence which is driven by the particles themselves.

$$t_{acc} \approx \kappa/u^2, \quad (3.13)$$

where $u =$ shock speed. Particles diffusing ahead of the shock excite Alfvén

waves which in turn reduce the scattering mean free paths to values approaching the gyro-radius so that the resulting diffusion coefficient takes a value close to the Bohm limit,

$$\kappa_B = \frac{1}{3} r_g v_p, \quad (3.14)$$

where κ_B = Bohm diffusion coefficient; r_g = particle gyro-radius and v_p = particle velocity (for relativistic particles $v_p \approx c$).

The cycle time depends on the diffusion coefficients upstream (κ_1) and downstream (κ_2) of the shock and on the shock velocity and compression ratio and is given by:

$$t_{cycle} \approx \frac{4}{c} \left(\frac{\kappa_1}{u_1} + \frac{\kappa_2}{u_2} \right), \quad (3.15)$$

and the acceleration time at energy E_1 defined by $E/(dE/dt)$, is then expressed as:

$$t_{acc} = \frac{4}{u_1} \left(\frac{\kappa_1}{u_1} + \frac{\kappa_2}{u_2} \right). \quad (3.16)$$

For a comprehensive treatment of these and other equations see Protheroe (1996).

In SNRs the relative orientation of the magnetic field and the shock front can be very diverse. For a spherically symmetric shock front expanding in a homogenous magnetic field for example, the directions of the shock normal and magnetic field change from parallel to perpendicular over the shock surface. For nearly perpendicular shocks, the acceleration process can

be very fast and effective due to reflections upstream (Naito & Takahara 1995). However, the velocity of the shock-magnetic field interaction in highly oblique shocks can approximate the light velocity, suppressing the injection efficiency of thermal particles which are essentially tied to magnetic field lines. The most effective injection is therefore most likely to occur in regions of SNRs where quasi-parallel shocks exist.

Chapter 4

Models of Shock Acceleration

4.1 The Test Particle Theory of Shock Acceleration

Much of the work done on the theory of shock acceleration in the late 1970s employed the test particle approach, whereby the plasma shock was a given phenomenon and the “test” particles were allowed to interact with it. In the test particle regime there is a simple relation between the spectrum of the accelerated particles and the jump conditions at the shock. This simple picture becomes complicated when the pressure of the accelerated particles (P_{CR}) becomes comparable with the pressure of the shocked fluid so that the non-linear backreaction of the particles becomes non-negligible and the spectrum is substantially affected.

The complicated effects, which seem to be important in several astrophysical situations, and lead to a highly non-linear problem, are often neglected, mainly because of the lack of an approach that allows to take them into account without the use of complicated numerical simulations which are usually of restricted use. As a result, in most of the applications of DSA to astrophysical simulations, the assumptions of test particles is adopted, even in those cases where this approximation works poorly.

4.1.1 Maximum Energy

A prediction of shock acceleration theory, at least in the test particle formalism, is that there is a maximum energy for the accelerated particles. In the case of SNR acceleration, Lagage & Cesarsky (1983) estimated the maximum energy of an ion of charge Z to be $\sim 10^{14}ZeV$. This prediction was not uniformly accepted however, with Jokipii for example showing that for quasi-perpendicular shocks the upper energy limit could be much larger.

The maximum energy of Fermi accelerated ions is of central importance to TeV observations. It can be determined in the Sedov phase of expansion of a SNR by equating the acceleration time to the remnant age (t_{SNR}) producing values of the order of (e.g. Baring et al 1997):

$$E_{max} \sim 4.7 \frac{r-1}{r} \frac{Q}{\eta} \left(\frac{B_1}{3\mu G} \right) \left(\frac{u}{1000 km/s} \right)^2 \frac{t_{SNR}}{10^3 yr} \text{ TeV}, \quad (4.1)$$

where B_1 = magnetic field in units of Gauss; u = expansion speed; $\eta = \lambda/r_g$.

In the Sedov phase, where the peak luminosity is expected (Drury et al. 1994), E_{max} is a slowly increasing function of time. For young SNRs early in the Sedov phase (200-5000 yrs), u is typically $\sim 200 - 3000$ km/s, implying age-limited acceleration terminating around 1-10 TeV.

Lagage & Cesarsky (1983) suggest two effects which may have an effect on limiting the energy gained by particles interacting with a SNR shock, namely the finite lifetime of the shock and the shock curvature. Although most scatterings occur either within the upstream or downstream region of the shock and do not change the particle energy, the few scatterings across the shock give an exponentially decreasing number of particles a momentum that increases exponentially with time. This results in a power-law distribution in momentum that cuts off due to the finite acceleration time. The cut-off momentum $p_{max}(t)$ advances with time as follows

$$\frac{dp_{max}}{dt} = \frac{p_{max}}{t_{acc}}, \quad (4.2)$$

with the acceleration time given by (e.g Axford 1981)

$$t_{acc} = \frac{3}{u_1 - u_2} \int_{p_{min}}^{p_{max}} \left[\frac{\kappa_1(p)}{u_1} + \frac{\kappa_2(p)}{u_2} \right] \frac{dp}{p}, \quad (4.3)$$

where u_1 and u_2 are the upstream and downstream flow speeds in the shock frame and κ_1 and κ_2 the particle diffusivities in the respective media. This

equation for t_{acc} with $\kappa = \kappa_B$ was found to be fast enough to explain the acceleration of CRs in SNRs up to the “knee” in the CR spectrum ($\sim 10^{15}$ eV) (e.g. Malkov et. al. 2001).

4.1.2 The Rankine-Hugoniot Relations

In a frame fixed with respect to the center of the explosion, the Rankine-Hugoniot jump conditions in the limit of a very strong shock can be expressed as

$$\rho_2 = \left(\frac{\gamma+1}{\gamma-1}\right)\rho_1, \quad u_2 = \frac{2}{(\gamma+1)}U_{sh}, \quad P_2 = \frac{2}{(\gamma+1)}\rho_1 U_{sh}^2. \quad (4.4)$$

If we know the value for U_{sh} , the above conditions yield the physical conditions just inside the blast wave:

$$\frac{\partial \rho}{\partial t} + \frac{1}{r^2} \frac{\partial}{\partial r} (r^2 \rho u) = 0, \quad (4.5)$$

$$\frac{\partial u}{\partial t} + u \frac{\partial u}{\partial r} = -\frac{1}{\rho} \frac{\partial P}{\partial r}, \quad (4.6)$$

$$\frac{\partial}{\partial t} \left[\rho \left(\varepsilon + \frac{1}{2} u^2 \right) \right] + \frac{1}{r^2} \frac{\partial}{\partial r} \left[r^2 \rho u \left(\varepsilon + \frac{P}{\rho} + \frac{1}{2} u^2 \right) \right] = 0, \quad (4.7)$$

with specific internal energy

$$\varepsilon = \frac{P}{(\gamma - 1)\rho}. \quad (4.8)$$

4.2 Magnetic Field

Since an ionized plasma has a high conductivity, any magnetic field present would be “frozen-in” to the plasma and contribute to the dynamics of the shock. In a parallel shock, where the magnetic field is parallel to the shock normal, the field’s only role is to support the Alfvén waves generated by the accelerated particles. In oblique shocks, the magnetic field takes a more active role and influences both the shock jump conditions and the particle acceleration. It has been observed (Candia et. al 2002) that at low energies, the CR particle diffusion is mainly due to small-scale turbulent fluctuations, while at higher energies the bulk of the CR diffusion is governed by the drifts that arise from the large-scale regular magnetic field, leading to significant large-scale asymmetries in the CR density distribution.

Taking a typical acceleration time given by

$$t_{acc} = \frac{3}{u_1 u_2} \left(\frac{\kappa_1 u_2 + \kappa_2 u_1}{u_1 - u_2} \right) \equiv 3 \left(\frac{\kappa_1 u_1 \left(\frac{1}{r} + \frac{1}{\tilde{r}} \right)}{\frac{u_1^3}{r} \left(1 - \frac{1}{r} \right)} \right) \quad (4.9)$$

where $r =$ compression ratio of shock (for a strong shock $r = 4$); $\tilde{r} =$ compression ratio of magnetic field ($\tilde{r} \in [1, 4]$); $u_2 = \frac{1}{4}u_1$ for a strong shock.

For a parallel shock with $\kappa_1 = \kappa_2$; $r = 4$; $\tilde{r} = 1$, we obtain an acceleration time of

$$t_{acc} = 20 \frac{\kappa_1}{u_1^2} \quad (\text{slow accelerator}). \quad (4.10)$$

For a perpendicular shock with $\kappa_2 = 1/4\kappa_1$; $r = 4$; $\tilde{r} = 4$

$$t_{acc} = 8 \frac{\kappa_1}{u_1^2} \quad (\text{fast accelerator}). \quad (4.11)$$

4.3 Models of Shock Acceleration

The main difficulty in numerical techniques to solve nonlinear diffusive shock acceleration is the fact that the diffusion-convection equation includes a wide range of length scales that need to be resolved. The diffusion-convection equation which describes the time evolution of the particle distribution $f(p, x, t)$, (e.g. Skilling 1975) takes the form;

$$\frac{df}{dt} = \frac{1}{3} \left(\frac{\partial u}{\partial x} \right) p \frac{\partial f}{\partial p} + \frac{\partial}{\partial x} (\kappa(x, p) \frac{\partial}{\partial x} f) + Q, \quad (4.12)$$

where Q = injection rate from thermal particles to CRs.

For a Bohm type diffusion where the scattering length is proportional to the particle momentum, the diffusion length increases linearly with momentum i.e. $L \propto p$. Considering the acceleration from supra-thermal particles ($p_{th}/m_p c \sim 10^{-3}$) to the “knee energy” ($p_{max}/m_p c \sim 10^6$) for exam-

ple, the ratio of the largest length scale to the smallest to be resolved is $L_{max}/L_{min} \sim 10^9$ (Kang 2000).

Berezhko et al. (1994) have developed a code to handle such a strong momentum dependent diffusion model in time-dependent simulations by introducing a “change of variables technique” in which the radial coordinate is transformed into a new variable scaled with particle diffusion length as

$$x(p) = \exp\left(-\frac{(r - R_S)}{L(p)}\right), \quad (4.13)$$

where $R_S =$ shock radius. This allowed them to solve the coupled system of gasdynamic equations and the CR transport equation even for a diffusion coefficient with a strong momentum dependence.

Prior to this, Krymsky & Pethukov (1980); Prishchep & Ptuskin (1981) and Drury (1982) studied solutions of the cosmic ray transport equation in blast waves from spherical explosions, making plausible assumptions regarding the velocity field behind the shock and the CR diffusion coefficient, while neglecting the CR pressure. However, even these simplified solutions do not express the CR spectrum throughout the whole downstream medium for arbitrary shock strength.

Because the acceleration process is inherently slow, particles take a long time to diffuse back and forth across the shock. Therefore, the energy gained by particles injected at the beginning of the SNR expansion and fortunate

enough to remain in the vicinity of the shock is limited. The diffusion coefficient of the CRs increases with energy. When the characteristic length of diffusion of the particles (of order κ/u_1 , where u_1 is the shock velocity) becomes comparable to the shock radius, the shock can no longer be considered plane. Particles interacting with a spherical shock lose some energy when travelling downstream and have the possibility of escaping upstream of the shock. As a result the acceleration mechanism can be totally/partially quenched.

In our treatment of shock acceleration we adopt a simplified approach which has been used successfully by many others (e.g. Bogdan & Völk 1983; Lagage & Cesarsky 1983; Völk & Biermann 1988; Ball & Kirk 1992; Protheroe & Stanev 1998) and which is often referred to as the “box” model.

In the following section I will outline the fundamentals of this model and its applications to shock acceleration in SNRs.

4.4 A Box Model of Shock Acceleration

The “box” model makes the simplified assumption that the particles being accelerated are uniformly distributed in a “box” extending one diffusion length either side of the shock. The accelerated particles have a differential energy spectrum $N(E)$ and gain energy at a rate $r_{acc}E$. However particles can also escape from the confines of the shock at a rate r_{esc} .

results in the following description of the acceleration:

$$\frac{\partial}{\partial t}[4\pi p^2 f L] + \frac{\partial \phi}{\partial p} = Q - U_2 4\pi p^2 f. \quad (4.16)$$

The first term on the left represents the time rate of change of the number of particles involved in the acceleration, the second term represents the divergence in the acceleration momentum flux. The first term on the right is a generic source term which can represent particles injected at the shock. The last term in the expression is the flux of particles advected downstream.

Substituting for ϕ in the above equation and simplifying we get a version of the box model as follows:

$$L \frac{\partial f}{\partial t} + U_1 f(p) + \frac{1}{3}(U_1 - U_2)p \frac{\partial f}{\partial p} = \frac{Q}{4\pi p^2}. \quad (4.17)$$

By making the following assumptions, we can simplify this equation further:

$$\dot{p} = \frac{p}{t_{acc}} \quad (4.18)$$

where

$$t_{acc} = \frac{3}{U_1 - U_2} L = \frac{3}{U_1 - U_2} \left(\frac{\kappa_1}{U_1} + \frac{\kappa_2}{U_2} \right). \quad (4.19)$$

$$\frac{\partial f}{\partial t} + \dot{p} \frac{\partial f}{\partial p} = \frac{Q}{4\pi p^2 L} - \frac{U_1}{L} f \quad (4.20)$$

$$\Leftrightarrow \frac{df}{dt} = \frac{Q}{4\pi p^2 L} - \frac{U_1}{L} f \quad (4.21)$$

which can be simplified to give

$$\Rightarrow df(p) = -\frac{U_1}{L} f(p) dt \quad (4.22)$$

for momenta above injection.

Chapter 5

Particle acceleration in supernova remnants and the Bell-Lucek hypothesis

5.1 Introduction

Bell and Lucek (2001) and Lucek and Bell (2000) have presented numerical simulations suggesting that the conventional process of particle acceleration in shocks, generally called diffusive shock acceleration, may also result in substantial amplification of the highly tangled magnetic field around the shock. We note in passing that this hypothesis provides a concrete physical mechanism for one of the many ideas of the late F. Hoyle who speculated (Hoyle

1960) that strong interstellar shocks might convert mechanical energy into roughly equal amounts of magnetic field energy, cosmic ray energy and thermal energy. Bell and Lucek suggest that this may enable strong supernova driven shocks in the interstellar medium to accelerate particles to energies well beyond what are conventionally held to be the maximum realistically attainable energies of a few times 10^{14} eV (e.g. Lagage and Cesarsky, 1983).

The Bell-Lucek hypothesis is of great interest because it is one of the few suggestions as to how the cosmic ray particles of energies at and above the “knee”, located at a few times 10^{15} eV, could be made in the Galaxy. It is therefore important to determine what the expected form of the source energy spectrum would be and whether the slight break in the observed spectrum at the “knee” can be accounted for in this way. There are also interesting implications for gamma ray observations of SNRs with the next generation of imaging atmospheric Cherenkov telescopes such as HESS. For an initial examination of this problem the so-called “box” models of particle acceleration offer enough accuracy and have the great advantage of computational simplicity.

5.2 The Bell-Lucek hypothesis

Bell and Lucek point out that in the conventional diffusive shock acceleration picture the energy density of the accelerated particles at and near the

shock front is extremely large, of order the total ram pressure of the incoming plasma, and thus much larger than the energy density of the magnetic field (the ratio of particle energy to field energy is of order the square of the shock Alfvén Mach number). The standard treatment of resonant wave excitation, in which the perturbations of the field are treated as Alfvén waves to lowest order and the interaction with the particles as a small perturbation, therefore becomes questionable. With the support of numerical simulations and simplified analytic models they suggest that in reality the field can be highly distorted by the particle pressure and wound up to the point where approximate equipartition holds.

If this amplified and distorted field is then used to estimate the particle diffusion in the shock neighbourhood, acceleration to substantially higher energies than in the conventional picture is obviously possible. Detailed estimates and simple dimensional analysis agree that the maximum particle rigidity is given, to order of magnitude, by the product of the field strength, the shock velocity and the shock radius, $BR\dot{R}$. Thus the increase is directly proportional to the increase in the field strength, which by the above argument is of order the Alfvén Mach number of the shock. This can easily be 10^3 for a young supernova remnant so that the effect is potentially very significant; acceleration to rigidities of a few 10^{17} eV, rather than the 10^{14} eV normally estimated, is easily possible.

5.3 Incorporating the Bell-Lucek effect in the “box” models

To get a first estimate of the effect of such a dynamically generated field on the acceleration we turn to the simplest treatment of shock acceleration, the so-called “box” model. In this the accelerated particles are assumed to be more or less uniformly distributed throughout a region extending one diffusion length each side of the shock, and to be accelerated upwards in momentum space at the shock itself with an acceleration flux

$$\Phi(p) = \frac{4\pi}{3} p^3 f(p) (U_1 - U_2) \quad (5.1)$$

per unit surface area where $f(p)$ is the phase space density of the accelerated particles (assumed to have an almost isotropic distribution). If the diffusion length upstream is L_1 , and that downstream is L_2 , then

$$L_1 \approx \frac{\kappa_1(p)}{U_1}, \quad L_2 \approx \frac{\kappa_2(p)}{U_2}, \quad (5.2)$$

where κ_1 and κ_2 are the upstream and downstream diffusion coefficients. To a first approximation we assume that both L_1 and L_2 are small relative to the radius of the shock and that we can neglect effects of spherical geometry (in fact it is not too difficult to develop a spherical box model, but it unnecessarily complicates the argument) so that the box volume is simply

$A(L_1 + L_2)$ where A is the surface area of the shock. The basic “box” model equation is then simply a conservation equation for the particles in the box; the rate at which the number in the box changes is given by the divergence of the acceleration flux in momentum space plus gains from injection and advection and minus advective losses to the downstream region.

$$\frac{\partial}{\partial t} [A(L_1 + L_2)4\pi p^2 f(p)] + \frac{A\partial\Phi}{\partial p} = AQ(p) + AF_1(p) - AF_2(p) \quad (5.3)$$

where $Q(p)$ is a source function representing injection at the shock (only important at very low energies), F_1 is a flux function representing advection of pre-existing particles into the system from upstream (normally neglected) and F_2 is the flux of particles advected out of the system and carried away downstream. The only complication we have to consider is that the box is time-dependent, with flow speeds, shock area and diffusion lengths all changing.

The escaping flux is determined simply by the advection across the downstream edge of the box, that is

$$F_2(p) = 4\pi p^2 f(p) \left(U_2 - \frac{\partial L_2}{\partial t} \right) \quad (5.4)$$

and the box equation simplifies, ignoring the $F_1(p)$ term, to

$$\frac{1}{A} \frac{\partial A}{\partial t} (L_1 + L_2) f + \frac{\partial L_1}{\partial t} f + (L_1 + L_2) \frac{\partial f}{\partial t} + U_1 f + (U_1 - U_2) \frac{p}{3} \frac{\partial f}{\partial p} = \frac{Q}{4\pi p^2} \quad (5.5)$$

5.4 Solution of the box equation

Partial differential equations of this form always reduce, by the method of characteristics, to the integration of two ordinary equations, one for the characteristic curve in the p, t plane

$$\frac{dp}{dt} = \frac{U_1 - U_2 p}{L_1 + L_2 3} \quad (5.6)$$

and one for the variation of f along this curve

$$(L_1 + L_2) \frac{df}{dt} + f \left[(L_1 + L_2) \frac{1}{A} \frac{\partial A}{\partial t} + \frac{\partial L_1}{\partial t} + U_1 \right] = \frac{Q}{4\pi p^2}. \quad (5.7)$$

Apart from at the injection momentum we can set $Q = 0$ and write the above equation as

$$\frac{d \ln f}{dt} = - \frac{1}{A} \frac{\partial A}{\partial t} - \frac{1}{L_1 + L_2} \frac{\partial L_1}{\partial t} - \frac{U_1}{L_1 + L_2}. \quad (5.8)$$

But the shock area A is a function only of time so that

$$\frac{\partial A}{\partial t} = \frac{dA}{dt} \quad (5.9)$$

and, although the upstream diffusion length does depend on both time and momentum, if we assume Bohm scaling for the two lengths so that

$$L \propto \frac{\kappa}{U} \propto \frac{pv}{UB} \quad (5.10)$$

(where v is the particle velocity) we can write

$$\frac{1}{L_1 + L_2} \frac{\partial L_1}{\partial t} = -\vartheta \frac{d \ln(U_1 B_1)}{dt} \quad (5.11)$$

where

$$\vartheta = \frac{L_1}{L_1 + L_2} \quad (5.12)$$

(obviously $0 < \vartheta < 1$). Finally, noting that

$$\frac{U_1}{L_1 + L_2} = \frac{3U_1}{U_1 - U_2} \frac{d \ln p}{dt} \quad (5.13)$$

and assuming that the compression ratio of the shock is fixed even if the shock speed changes, we can simplify the equation to

$$\frac{d \ln f}{dt} = -\frac{d \ln A}{dt} + \vartheta \frac{d \ln(U_1 B_1)}{dt} - \frac{3U_1}{U_1 - U_2} \frac{d \ln p}{dt} \quad (5.14)$$

which integrates trivially to relate the value of f at the end of one of the characteristic curves, say at the point (p_1, t_1) , to the value at the start, say

at (t_0, p_0) , as follows;

$$\frac{f(t_1, p_1)}{f(t_0, p_0)} = \left(\frac{A(t_1)}{A(t_0)} \right)^{-1} \left(\frac{U_1(t_1)B_1(t_1)}{U_1(t_0)B_1(t_0)} \right)^{\theta} \left(\frac{p_1}{p_0} \right)^{-3U_1/(U_1-U_2)} \quad (5.15)$$

This rather beautiful result shows how the standard test particle power-law is modified by what is essentially a geometrical dilution effect as the box volume changes. The amplitude varies inversely as the shock area and also decreases if the upstream diffusion length (at fixed energy) increases, but with an exponent between zero and one determined by the ratio of the upstream diffusion length to the total width of the diffusion region. It is very interesting that the result is not simply a variation inversely as the box volume, which one might naively expect. This reflects the fundamental asymmetry between the upstream and downstream regions, that upstream is empty outside the diffusion region whereas the entire downstream region is filled with accelerated particles.

If we assume pure Bohm scaling the other differential equation is also integrable so that the problem is reduced entirely to quadratures (of course only within the various approximations we are making; but still a remarkable result). Bohm scaling implies that the mean free path is of order and proportional to the particle gyroradius, so that if the particle charge is e

$$L_1 + L_2 \approx \alpha \frac{pv}{3eB_1U_1} \quad (5.16)$$

where α is a dimensionless parameter (probably of order ten). Substituting in the equation of the characteristic we get

$$v \frac{dp}{dt} = \frac{1}{\alpha} (U_1 - U_2) U_1 e B_1 \quad (5.17)$$

and noting the relativistic identity between kinetic energy T , momentum p and velocity v ,

$$v = \frac{dT}{dp} \quad (5.18)$$

we can integrate this as

$$T_1 - T_0 = \frac{e}{\alpha} \int_{t_0}^{t_1} (U_1 - U_2) U_1 B_1 dt. \quad (5.19)$$

For relativistic particles the kinetic energy and the momentum are essentially interchangeable with $T = c\sqrt{p^2 + m^2c^2} - mc^2 \approx cp$.

These two integrals together reduce the problem of calculating the final spectrum to that of determining the initial amplitude $f(t_0, p_0)$ which in turn depends on the injection rate and its time dependence.

5.5 The injection rate

There are two main approaches to the injection rate. The simplest, which is perhaps more consistent with the test particle approach, is to simply parametrise it by assuming that some fraction of the incoming thermal par-

ticles are “injected” as non-thermal particles at some suitably chosen “injection momentum” which separates the thermal particle population from the non-thermal. In other words one writes

$$Q(p, t) = \eta(t)n_1U_1\delta(p - p_{\text{inj}}(t)) \quad (5.20)$$

where n_1 is the upstream thermal particle number density, $\eta \ll 1$ is the injection fraction, p_{inj} is the injection momentum and as usual δ is Dirac’s delta distribution. It should be clear that this is a parametrisation rather than a true injection model, however it, or equivalent parametrisations, have been very widely used, typically with η taken to be a constant of order 10^{-5} to 10^{-4} for protons and $p_{\text{inj}} \approx 10m_pU_1$ where m_p is the proton mass. However there is no real justification for this apart from the fact that it seems to yield reasonable results in many cases.

With the above parametrisation the distribution function just above the injection energy can be simply determined by equating the acceleration flux to the injection flux,

$$\frac{4\pi p_{\text{inj}}^3}{3} (U_1 - U_2) f(p_{\text{inj}}) = \eta n U_1 \quad (5.21)$$

giving

$$f(p_{\text{inj}}) = \frac{3}{4\pi p_{\text{inj}}^3} \frac{U_1}{U_1 - U_2} n \eta. \quad (5.22)$$

The second approach adopts the idea, which can be traced back to the early work of Eichler, that the injection process is inherently extremely efficient

but that various feedback processes operate to reduce it to the point where the accelerated particles carry a significant part of the energy dissipated in the shock. Probably the most sophisticated modern version of this idea is to be found in the papers by Malkov (refs). This, or something similar, is in fact required for the Bell-Lucek hypothesis to operate because it requires the accelerated particle energy density to be substantial and of order the ram pressure of the upstream flow. For a standard spectrum close to p^{-4} the energy is almost uniformly distributed per logarithmic interval over the relativistic part of the spectrum. This suggests taking a reference momentum in the transrelativistic region, $p_0 \approx mc$, and determining f by a relation of the form

$$\frac{4\pi p_0^3}{3} f(p_0) mc^2 \approx \beta \rho U_1 (U_1 - U_2) \quad (5.23)$$

where β is a number which depends logarithmically on the upper cut-off and which for supernova remnants is probably somewhere between 10^{-1} and 10^{-2} . It should be noted that very little work has been done on the problem of electron injection, despite its obvious importance for observational tests.

5.6 Application to the Sedov solution

Let us now apply these ideas to the Sedov solution (also studied by Taylor and von Neumann) for a strong spherical explosion in a cold gas where the shock radius $r \propto t^{2/5}$ and the shock velocity decreases as $U \propto t^{-3/5}$. On the

Bell-Lucek hypothesis the magnetic field also scales as the shock velocity, $B \propto t^{-3/5}$ and thus the characteristic acceleration curves are given by

$$T_1 - T_0 \propto \int_{t_0}^{t_1} (U_1 - U_2) U_1 B dt \propto \int_{t_0}^{t_1} t^{-9/5} dt \propto t_0^{-4/5} - t_1^{-4/5}. \quad (5.24)$$

These curves all rise extremely steeply, representing an initial phase of rapid acceleration, turn over and then become asymptotically flat. Physically it is clear that, as the shock slows and the field drops, the high energy particles cease to be significantly accelerated and simply diffuse further and further in front of the shock. In fact in reality they should probably be thought of as decoupling from the shock and forming part of the general interstellar population at this point, but within the box model they simply fill a steadily growing upstream region. We will return to this point later.

A very important aspect of the curves is that they uniquely relate final energies (or equivalently momenta) to starting times. Asymptotically the relation is a simple power-law; for $T_1 \gg T_0$ and $t_0 \ll t_1$ we have simply

$$p_1 \propto T_1 \propto t_0^{-4/5}, \quad t_0 \propto p_1^{-5/4}. \quad (5.25)$$

Using this we can translate the geometrical dilution factors to additional power-law terms in the final momentum. Explicitly, a given final momentum

maps to a starting radius

$$r_0 \propto t_0^{2/5} \propto p_1^{-1/2} \quad (5.26)$$

and thus the surface area factor translates to a p_1^{-1} factor,

$$\left(\frac{A(t_1)}{A(t_0)}\right)^{-1} \propto p_1^{-1} \quad (5.27)$$

Similarly, the factor deriving from the upstream diffusion scale depends on the shock velocity

$$U \propto t^{-3/5} \propto p_1^{3/4} \quad (5.28)$$

and the magnetic field, which on the Bell-Lucek hypothesis scales as U , giving another $p_1^{3/4}$ factor, all raised to the power ϑ giving a final factor

$$[U_1(t_0)B_1(t_0)]^{-\vartheta} \propto p_1^{-3\vartheta/2} \quad (5.29)$$

Finally, we need to determine the initial amplitude of f from an injection model. If we use the η parametrisation

$$p_{\text{inj}} = p_0 \propto U(t_0) \propto p_1^{3/4} \quad (5.30)$$

and

$$f_0 \propto \eta n p_0^{-3}. \quad (5.31)$$

Assuming the standard shock compression $U_1/U_2 = 4$ so that $3U_1/(U_1 - U_2) = 4$ we thus get, at fixed t_1 and varying the final energy or momentum p_1 ,

$$f(p_1) \propto \eta m_0 p_0^{-3} A(t_0) [U_1(t_0) B_1(t_0)]^{-\vartheta} \left(\frac{p_1}{p_0}\right)^{-4} \propto \eta p_1^{3/4} p_1^{-1} p_1^{-3\vartheta/2} p_1^{-4} \quad (5.32)$$

so that, if η is constant, the slope is steepened from the canonical value of 4 to

$$4.25 + \frac{3\vartheta}{2}. \quad (5.33)$$

If we use the alternative ‘‘equipartition’’ argument that f_0 should be dynamically determined in the transrelativistic region we have $p_0 \approx mc$ independent of p_1 and

$$f(p_0) \propto U_1^2 \propto r^{-3} \propto p_1^{3/2} \quad (5.34)$$

giving

$$f(p_1) \propto p_1^{3/2} p_1^{-1} p_1^{-3\vartheta/2} p_1^{-4} \quad (5.35)$$

so that the slope is now

$$4 + \frac{3\vartheta - 1}{2}. \quad (5.36)$$

It is interesting that because of the strong injection at early times this model can even, if $\vartheta < 1/3$, lead to a slight flattening of the spectrum. However, especially at high energies, it is unlikely that the upstream diffusion region could be so small and a modest steepening of the spectrum is more likely.

These results refer of course only to the asymptotic behaviour of the high

energy part of the spectrum. As p_1 is decreased there comes a point where t_0 is no longer small relative to t_1 . At this point all values of the final momentum map down to a small approximately constant region and the spectrum becomes simply the standard p^{-4} spectrum. The conclusion therefore is that on the Bell-Lucek hypothesis the spectrum accelerated by a Sedov-like shock should exhibit a spectral break at the energy determined by the current acceleration cut-off energy below which one observes the standard shock acceleration spectrum, but above which a slightly different power-law continues to higher energies.

5.7 Conclusions

Obviously further and more detailed work is needed, but it is very encouraging that even such a simple model can produce spectra remarkably close to the inferred cosmic ray source spectrum through the “knee” region. In fact we are not aware of any other acceleration model that can naturally produce a break of the right magnitude (about 0.5 in the exponent) at the right position (modulo major uncertainties in interstellar propagation at these energies of course).

Malkov et al. (2000) recently suggested a so-called self-organised critical (SOC) level, whereby the shock modification follows rather abruptly after the maximum momentum has passed through the critical value, so that crucial

acceleration parameters such as the maximum momentum and injection rate are driven back to their critical values, limiting shock modification and setting it at some marginal level. (See also Jones 2000; Malkov & Drury 2001; Malkov & Diamond 2001, for more discussions of the critical interrelation between the injection, maximum energy and shock structure).

Malkov et al. (2001) also addressed the issue of particle acceleration by SNRs in an attempt to determine what happens to the particle spectrum provided the acceleration is indeed fast enough to access TeV energies over the lifetime of the SNRs in question, and suggested a possible reason for the lack of detection of TeV protons in SNRs.

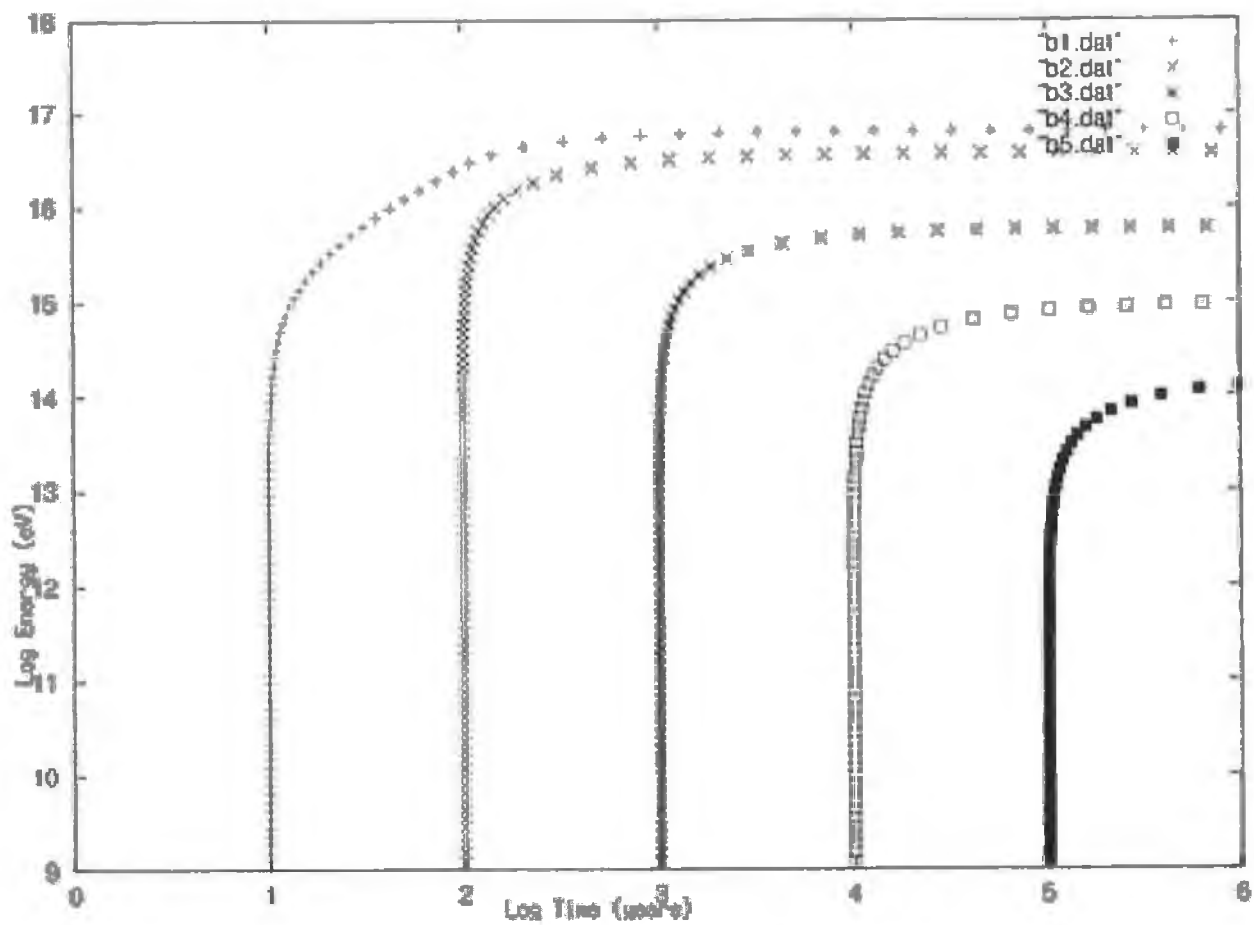


Figure 5.1: *Log Energy (eV) versus Log Time (years) for typical protons in the box*

Chapter 6

Discussion and Future Work

It appears that SNR shocks in the winds from supernova progenitor stars can produce particles at least up to the “knee” of the observed CR spectrum. Most successful observations have been made for CR electrons. Many SNRs are observed by radio synchrotron radiation due to relativistic electrons gyrating around a magnetic field. In some remnants, this synchrotron radiation extends to X-rays, e.g. SN 1006 which emits synchrotron X-ray radiation at two bright rims where the X-ray energy spectrum is a power-law, a typical signature of synchrotron emission. The maximum electron energy emitting this radiation was estimated to be 100 TeV, consistent with the predictions of the standard model. Relativistic electrons can also be detected in γ -rays by nonthermal Bremsstrahlung and by inverse Compton scattering of the cosmic microwave background radiation. The TeV γ -rays from Sn

1006 detected by the CANGAROO experiment are believed to be due to the inverse Compton scattered cosmic microwave background radiation from 40 TeV electrons (Taniomori et al. 1998). Detection of CR protons in SNRs however, has been discouraging to date. Relativistic protons collide with the ISM and emit γ -rays via pion decay. According to theoretical estimates, the detection of pion decay gamma-rays from nearby SNRs may be difficult with current detectors but not impossible (Drury et al. 1994, Berezhko & Völk 2000). In many cases, gamma-ray observations have only given upper limits without any positive detections.

It is thought that if some of the unidentified EGRET source detections turn out to be of gamma-rays emitted in the environs of remnant shells, then γ -ray emitters must be a minority of remnants, possibly mostly young, given that they cannot produce ions above a few TeV. Remnants that provide CRs up to the knee in the spectrum must therefore be a gamma-ray quiet majority. Alternatively, if fluxes of shell origin are well below EGRET and Whipple's flux sensitivities, then the notion that shell-type remnants are simultaneously gamma-ray bright and prolific producers of CRs becomes tenable. It has therefore become evident that the Whipple and HEGRA upper limits have not destroyed the hypothesis that shocks in shell-type remnants energize the particles responsible for the gamma-ray emission, but rather have provided a powerful tool for constraining our understanding (e.g. Baring et al. 1997). Given detections of Sn 1006 by CANGAROO, it is expected that in future, coupled TeV/sub-GeV, MeV and X-ray observations

will refine our understanding of gamma-ray SNRs.

The lack of proton detection calls for further improvements on theoretical modelling and numerical calculations as well as experimental sensitivity. A true progress in modelling particle acceleration in actual sources requires a full plasma non-linear description, including feedback of accelerated particles at the turbulent wave fields near the shock wave, flow modification caused by the CRs plasma pre-shock compression and, of course, the appropriate boundary conditions.

It is hoped that the advent of more sensitive ground-based detectors such as the HESS array, will provide an experimental basis for an improved understanding of the acceleration, propagation and interactions of the nonthermal populations of particles discussed above. At this time only a handful of TeV gamma-ray sources have been established. Examples include a few active galaxies, a few supernova remnants, and pulsar nebulae. With such small samples, and data sets of very limited statistical precision, it is difficult to impossible to differentiate between generic features of the sources and the acceleration mechanisms, and specific characteristics of individual objects. The goal of instruments such as HESS is to detect a sufficient number of sources of each type to allow a meaningful taxonomy of sources and a classification of the acceleration mechanisms.

Bibliography

- [1] Axford, W.I., Leer, E., Skadron, G., 1977, Proc. 15th. International Cosmic Ray Conference, **11**, 132
- [2] Axford, W.I., 1981, Proc. 10th. Texas Symp. Relativistic Astrophys. (Baltimore: Ann. NY Acad. Sci) **375**, 297-313
- [3] Ball, L., Kirk, J.G., 1992, ApJ., **396**, 39-42
- [4] Baring, M.G., Ellison, D.C., Grenier, I.A., 1997, Proc. Monorid. Workshop on VHE Phenomena in the Universe
- [5] Baring, M.G., et al. 1997, astro-ph/9711257
- [6] Baring, M.G., 1999, AIP Conf. Proc. 515, Towards a Major Atm. Cerenkov Detector VI, Snowbird Utah
- [7] Bell, A.R., 1978, MNRAS **182**, 147
- [8] Bell, A.R., Lucek, S.G., 2001, MNRAS, **321**, 433
- [9] Berezhko, E.G., Völk, H.J., 2000, Astron. Astrophys., **357**, 283

- [10] Berezhko, E.G., Ksenofontov, L.T., Yelshin, V.K., 1994, *Astropart. Phys.*, **2**, 215
- [11] Biermann, P.L., 1993, *Inv. Rap. High. Papers* 45, 23rd ICRC Calgary
- [12] Blandford, R.D., Ostriker, J.P., 1978, *ApJ.*, **221**, L29
- [13] Blasi, P., 2001, *astro-ph/0104064*
- [14] Blondin, J.M., Wright, E.B., Borkowski, K.J., Reynolds, S.P., 1998, *ApJ.*, **500**
- [15] Bogdan, T.J., Völk, H.J., 1983, *Astron. Astrophys.*, **122**, 129-136
- [16] Candia, J., Roulet, E., Epele, L.N., 2002, *Astro. Phys.* **17** 23
- [17] Cioffi, D.F., McKee, C.F., Bertschinger, E., 1988, *ApJ.*, **334**, 252
- [18] Cocconi, G., 1960, *Moscow CR Conf.* II 309
- [19] Chadwick, P.M. et al., 1999, *AIP Conf. Proc.* 515, *Towards a Major Atm. Cerenkov Detector VI, Snowbird Utah*
- [20] Drury, L.O'C., Völk, H., 1981, *ApJ.*, **248**, 344-351
- [21] Drury, L.O'C., 1983, *Rep. Prog. Phys.*, **46**, 973
- [22] Drury, L.O'C., Duffy, P., Völk, H., 1994, *astro-ph/9408012*
- [23] Drury, L.O'C., Aharonian, F., Völk, H., 1994, *Astron. Astr.*, **287**, 959

- [24] Drury, L.O'C., Keane, A.J., 1995, Nucl. Phys. B, 39A 165
- [25] Drury, L.O'C., Duffy, P., Eichler, D., Mastichiadis, A., 1999, Astron. Astrophys., **347**, 370-374
- [26] Drury, L.O'C., Kirk, J., Duffy, P., 1999, AIP Conf. Proc. 515, Towards a Major Atm. Cerenkov Detector VI, Snowbird Utah
- [27] Fermi, E., 1949, Phys. Rev., **75**, 1169
- [28] Fichtel, C.E., Linsley, J., 1986, ApJ., **300**, 474
- [29] Friedhandler, M.W., *Cosmic Rays*, 1989, Harvard University Press
- [30] Gaisser, T.K., *Cosmic Rays and Particle Physics*, 1990, Cambridge University Press
- [31] Gaisser, T.K., Protheroe, R.J., Stanev, T., 1996, astro-ph/9609044 v2
- [32] Gaisser, T.K., Protheroe, R., Stanev, T., 1998, ApJ., **492**, 219
- [33] Galbraith, W., Jelley, J.V., 1995, J. Atmos. & Terrestrial Phys. **6**, 250; 304
- [34] Gieseler, U.D.J., Jones, T.W., Kang, H., 2000, astro-ph/0011058
- [35] Grenier, I.A., 1999, AIP Conf. Proc. 515, Towards a Major Atm. Cerenkov Detector VI, Snowbird Utah
- [36] Hoyle, F., Fowler, W.A., 1960, ApJ., **132**, 565

- [37] Jelley, J.V., Porter, N.A., 1963, Quarterly J. of the R.A.S., **4**, 275
- [38] Jokipii, J.R., Morfill, G.E., 1986, ApJ., **312**, 170
- [39] Jones, T.W., 2000, astro-ph/0012483
- [40] Kang, H., 2000, astro-ph/0012495
- [41] Karakula, S., Tkaczyk, W., 1993, Astro. Phys. **1**, 229
- [42] Kirk, J.G., Melrose, D.B., Priest, E.R., *Plasma Astrophysics Saas-Fee Advanced Course 24, Lecture Notes 1994*, Swiss Society for Astrophysics and Astronomy, 1994, Springer-Verlag
- [43] Kirk, J.G., Dendy, R.O., 2001, astro-ph/0101175
- [44] Kobayakawa, K., Sato, Y., Samura, T., astro-ph/0008209
- [45] Konopelko, A., Pühlhofer, G., 1999, AIP Conf. Proc. 515, Towards a Major Atm. Cerenkov Detector VI, Snowbird Utah
- [46] Krymsky, G.F., 1977, Dok. Acad. Nauk. USSR, **234**, 1306
- [47] Krymsky, G.F., Petukhov, S.I., 1980, Dis. Astron. Zh., **6**, 227 (Engl. transl., Sov. Astron. Lett., **6**, 124)
- [48] Lagage, P.O., Cesarsky, C.J., 1983, Aston. Astr., **118**, 223; **125**, 249
- [49] Lagutin, A.A., Uchaikin, V.V., 2001, Proc. ICRC 2001

- [50] Lamb, R.C., Macomb, D.J., 1999, AIP Conf. Proc. 515, Towards a Major Atm. Cerenkov Detector VI, Snowbird Utah
- [51] Landau, L.D., Lifshitz, E.M., *Fluid Mechanics, 2nd. Edition Landau and Lifshitz Course of Theoretical Physics Volume 6*, 1987, Pergamon Press
- [52] Longair, M.S., *High Energy Astrophysics Volume 2*, 1981, Cambridge University Press
- [53] Lucek, S.G., Bell, A.R., 2000, MNRAS **314**, 65
- [54] Lucek, S.G., Bell, A.R., 2000, MNRAS **321**, 433-438
- [55] Malkov, M.A., 1987, ApJ., **485**, 638
- [56] Malkov, M.A., Diamond, P.H., Völk, H.J., 2000, ApJ., **533**, L171
- [57] Malkov, M.A., Drury, L.O'C., 2001, Rep. Prog. Phys., **64**, 429
- [58] Malkov, M.A., Diamond, P.H., Jones, T.W., 2001, Proc. ICRC 2001
- [59] Malkov, M.A., Diamond, P.H., Jones, T.W., 2002, ApJ., **571**, 856-865
- [60] Marcowith, A., Kirk, J.G., 1999, astro-ph/9905176
- [61] Mastichiadis, A., de Jager, O., 1996, Astron. Astro., **311**, 15
- [62] McKee, C.F., 1974, ApJ., **188**, 335
- [63] McKee, C.F., Truelove, J.K., 1995, Phys. Rep., **256**, 157

- [64] Miniati, F., 2002, astro-ph/0203014
- [65] Moraal, H., Axford, W.I., 1983, *Astron. Astrophys.* **125**, 204-216
- [66] Naito, T., Takahara, F., 1995, *MNRAS*, **275**, 1077
- [67] Ostrowski, M., 2001, astro-ph/0104120
- [68] Press, W.H., Teukolsky, S.A., Vetterling, W.T., Flannery, B.P.,
Numerical Recipes in C Second Edition, 1999, Cambridge University
Press
- [69] Prishchep, V.L., Ptuskin, V.S., 1981, *Astron. Zh.*, **58**, 779 (Engl. transl.,
Sov. Astron., **25**, 446)
- [70] Protheroe, R.J., 1996, astro-ph/9612212
- [71] Protheroe, R.J., Stanev, T., 1998, astro-ph/9808129
- [72] Ptuskin, V.S., et al., 1993, *Astron. Astrophys.*, **268**, 726
- [73] Ramakrishnan, A., *Elementary Particles and Cosmic Rays*, 1962,
Pergamon Press
- [74] Rao, M.V.S., Sreekanten, B.V., *Extensive Air Showers*, 1998, World
Scientific Publishing Co. Pte. Ltd.
- [75] Rowell, G.P. et al., 1999, AIP Conf. Proc. 515, Towards a Major Atm.
Cerenkov Detector VI, Snowbird Utah

- [76] Schlickeiser, R., 1984, *Astron. Astrophys.*, **136**, 227-236
- [77] Shu, F.M., *The Physics of Astrophysics, Volume II Gas Dynamics*, 1992, University Science Books
- [78] Simpson, J., 1983, *Ann. Rev. Nucl. Particle Sci.*, **33**, 323
- [79] Sinitsyna, V.G., 1999, *AIP Conf. Proc.* 515, Towards a Major Atm. Cerenkov Detector VI, Snowbird Utah
- [80] Skilling, J., 1975, *MNRAS*, **172**, 557
- [81] Spitzer, L., Jr., *Physical Processes in the ISM*, 1978, Wiley-Interscience
- [82] Sturmer, S.J., Skibo, J.G., Dermer, C.D., Mattox, J.R., 1997, *ApJ.*, **490**, 619
- [83] van der Swaluw, E., *Supernova Remnants, Pulsar Wind Nebulae and Their Interaction*, 2001, PhD Thesis
- [84] Taniomori, T., et al., 1998, *ApJ.*, **497**, L25
- [85] Völk, H.J., Biermann, P.L., 1988, *ApJ.*, **333**, 65-68
- [86] Völk, H.J., 1999, *AIP Conf. Proc.* 515, Towards a Major Atm. Cerenkov Detector VI, Snowbird Utah
- [87] Völk, H.J., 1999, *AIP Conf. Proc.* 515, Towards a Major Atm. Cerenkov Detector VI, Snowbird Utah

- [88] Wilson, J.G., Wouthuysen, S.A., *Progress in Elementary Particle and Cosmic Ray Physics*, 1967, North-Holland Publishing Company
- [89] Woltjer, L., 1972, *ARA & A*, **10**, 129
- [90] Yoshikoshi, T., 1999, *AIP Conf. Proc.* 515, Towards a Major Atm. Cerenkov Detector VI, Snowbird Utah
- [91] Zatsepin, G.T., Chudakov, A.E., 1961, *Zh. Eksp. Teor. Fiz.*, **41**, 655

Appendix A

```
# include <stdio.h>
# include <math.h>

double tsw, xsw, U0, B0;
/* global constants for simple SNR model */

FILE      *fp;

double rk4(double y, double dydx, double x, double h);
/* does one rk4 step */
void rk4umb(double ystart, double xstart, double xend, int nstep);
/* takes nsteps of rk4 from xstart to xend */

/* -----
With  $y=\ln(p)$ ,  $x=\ln(t)$  the ODE to integrate is

$$\frac{dy}{dx} = \frac{t}{3} \{U_1 - U_2 \over L_1 + L_2\}$$

\propto  $U^2 B \frac{t}{p}$ 
with  $t=\exp(x)$  and  $U$  and  $B$  given functions of  $t$ .
The const is of order  $3 \cdot 10^{-4}$  if we measure  $t$  in years,  $p$  in eV/c
 $U$  in km/s and  $B$  in nT giving fast initial acceleration to
```

about 10^{17} eV

----- */

```
double derivs(double x, double y)
{
    double t, p, U, B;
    t = exp(x*M_LN10);
    p = exp(y*M_LN10);
    /* For the moment just use very simple model for U1 = Shock speed
    and amplified magnetic field B */
    if ( t<tsw )
        {U = U0;
        B = B0;}
    else
        {U = U0 * exp(-0.6*(x-xsw)*M_LN10);
        B = B0 * U/U0;}
    return 30000.0*U*U*B*t/p;
};
```

```
/* Algorithm rk4 to perform one step of integration */
```

```
double rk4(double y, double dydx, double x, double h)
```

```
{
```

```

double xh, hh, h6, dym, dyt, yt, yout;

hh = h * 0.5;
h6 = h / 6.0;
xh = x + hh;
yt = y + hh * dydx; /* First step */
dyt = derivs(xh, yt); /* Second step */
yt = y + hh * dyt;
dym = derivs(xh, yt); /* Third step */
yt = y + h * dym;
dym += dyt;
dyt = derivs(x + h, yt); /* Fourth step */
return yout = y + h6*(dydx + dyt + 2.0 * dym); /* Adding increments */
}

/* Driver routine rk4 that takes nstep RK4 steps from xstart to xend */

void rk4(double ystart, double xstart, double xend, int nstep)
{
int k;
double x, y, dydx, yout, h;

y = ystart;

```

```

x = xstart;
while(x<xend)
{
dydx = derivs(x, y);
h = 0.1/dydx;
if (h>0.2) {h=0.2;};
y = rk4(y, dydx, x, h);
x += h;
fprintf(fp, "%lf %lf\n", x, y);
};
}

int main()
{
int i, nstep;
double ystart, xstart, xend;

/* Initialise */
tsw = 100; /* sweep-up at 100 years */
xsw = log10(tsw);
U0 = 10000; /* initial ejecta velocity in km/s */
B0 = 100; /* initial amplified field in nT */

```

```

/* Open output file */
fp=fopen("b3.dat","w");

/* Read in parameters */
printf("Enter value for log10 initial time: \n");
scanf("%lf", &xstart);
printf("Enter value for log10 end time: \n");
scanf("%lf", &xend);
printf("Enter value for log10 initial energy (in eV): \n");
scanf("%lf", &ystart);
printf("Integrating from %g to %g; ystart %g\n", xstart, xend, ystart);

rkdumb(ystart, xstart, xend, nstep);

fclose(fp);
return 0;
}

```